Comprehensive Review

The Science of Conventional and Water-Cooled Monopolar Lumbar Radiofrequency Rhizotomy: An Electrical Engineering Point of View

Richard D. Ball, MD, PhD

From: Neuromuscular and Rehabilitation Associates of Northern Michigan, Traverse City, MI.

Address Correspondence:
Richard D. Ball, MD, PhD
Neuromuscular and Rehabilitation Associates of Northern Michigan
3988 W. Royal Dr.
Traverse City, MI 49684-9200
E-mail: r.d.ball@charter.net

Disclaimer: There was no external funding in the preparation of this manuscript. Conflict of interest: The author certifies that he, or a member of his immediate family, has no commercial association (i.e., consultancies, stock ownership, equity interest, patent/licensing arrangements, etc.) that might post a conflict of interest in connection with the submitted manuscript.

Manuscript received: 11-21-2012
Revised manuscript received: 05-23-2013
Accepted for publication: 07-16-2013

Free full manuscript: www.painphysicianjournal.com

Radiofrequency ablation (RFA) is a safe and effective pain therapy used to create sensory dysfunction in appropriate nerves via thermal damage. While commonly viewed as a simple process, RF heating is actually quite complex from an electrical engineering standpoint, and it is difficult for the non-electrical engineer to achieve a thorough understanding of the events that occur. RFA is highly influenced by the configuration and properties of the peri-electrode tissues. To rationally discuss the science of RFA requires that examples be procedure-specific, and lumbar RFA is the procedure selected for this review. Adequate heating of the lumbar medial branch has many potential failure points, and the underlying science is discussed with recommendations to reduce the frequency of failure in heating target tissues. Important technical details of the procedure that are not generally appreciated are discussed, and the status quo is challenged on several aspects of accepted technique. The rationale underlying electrode placement and the limitations of RF heating are, for the most part, commonly misunderstood, and there may even need to be significant changes in how lumbar radiofrequency rhizotomy (RFR) is performed. A new paradigm for heating target tissue may be of value. Foremost in developing best practices for this procedure is avoiding pitfalls. Good RF heating and medial branch lesioning are the rewards for understanding how the process functions, attention to detail, and meticulous attention to electrode positioning.

Key words: Electrical equipment and supplies, zygapophyseal joint, catheter ablation, lumbar vertebrae, low back pain, lumbar vertebrae/innervation, radiofrequency ablation, water-cooled radiofrequency ablation, conventional radiofrequency ablation, radiofrequency electrode behavior

Pain Physician 2014; 17:E175-E211

Radiofrequency ablation (RFA) is a well-established technique used to produce thermal tissue damage to treat cardiac arrhythmias (1), neoplasms (2-6), and chronic pain (7-23).

Numerous attempts have been made to reduce the behavior of RF electrodes to tables describing the size of the lesion associated with a given electrode heated for a specific time at a specific target temperature (24,25). Radiofrequency electrode behavior cannot be simplified this easily, but these tables do contain some useful information.

This review discusses, from an electrical engineering viewpoint, RFA of the lumbar medial branch (MB), aka radiofrequency rhizotomy (RFR), impairing pain transmission from structures innervated by this nerve, not just the facet joints. Since the configuration and properties of the peri-electrode tissues are the single most important determinant of electrode behavior, it is imperative to discuss RF electrode behavior in the context of a specific procedure, and lumbar RFR has been chosen for this review. The primary efficacy of RFA presumably reflects heat-induced damage. Other processes may be involved, including electroporation (26-31), where

cell membrane permeability is rendered abnormal by excessive trans-membrane voltages. Additionally, RF heating may damage the vascular supply to the nerve, the Schwann cells, or otherwise disorder its physiology. This review focuses purely on conventional and water-cooled monopolar, not bipolar, RFA. Monopolar water-cooled RFA is simply a special case of conventional RFA that ameliorates some technical issues limiting maximum applied RF power, but is not a panacea or fundamentally different technique (32-39). The biophysical concepts underlying RFA are complicated, but this review is primarily descriptive and based on fundamental concepts and empirical observations. More detailed theoretical explanations of the basic phenomena involved are available elsewhere (40-48). Basic definitions and formulas relevant to RFA are summarized in Appendices A and B.

RF Electrode Structure

The structure of essentially all conventional interventional pain management (IPM) RFR electrodes are comparable, being metal cylinders of variable length (2.5 mm-10 mm) and diameter (16G-22G). The water-cooled electrode (4.5 mm-5.5 mm x 17G) is also shown. Figure 1 shows stylized drawings of these electrodes.

Basic RF Electrode Behavior

Heat and Temperature

Radiofrequency electrode behavior can be summarized in that heat is produced when adequate RF current is passed through tissue having sufficient impedance. The total heat generated (joules) is equal to the average power input (watts) multiplied by time. The temperature rise of the tissue is equal to the total heat adsorbed divided by the total heat capacity. Because of its low intrinsic impedance, the RF electrode is not directly heated by the RF current, but rather is heated by the surrounding tissues. Only in the immediate region of the ablation electrode does the RF current density reach levels that produce significant heating. The surface area of a 10 mm, 18G ablation electrode is 3.8 mm^2, and the surface area of a typical grounding pad is 10,000 mm^2, yielding a current density (j) ratio of over 2,600. Since heating/power is proportional to j^2, the power ratio/mm^2 is over 6 x 10^6. Due to the tissue geometry, j^2 remains low until only a few mm away from the ablative electrode. Therefore, only the immediate area of the ablative electrode need be considered in analyzing RF electrodes.

The temperature required to lesion the target tis-

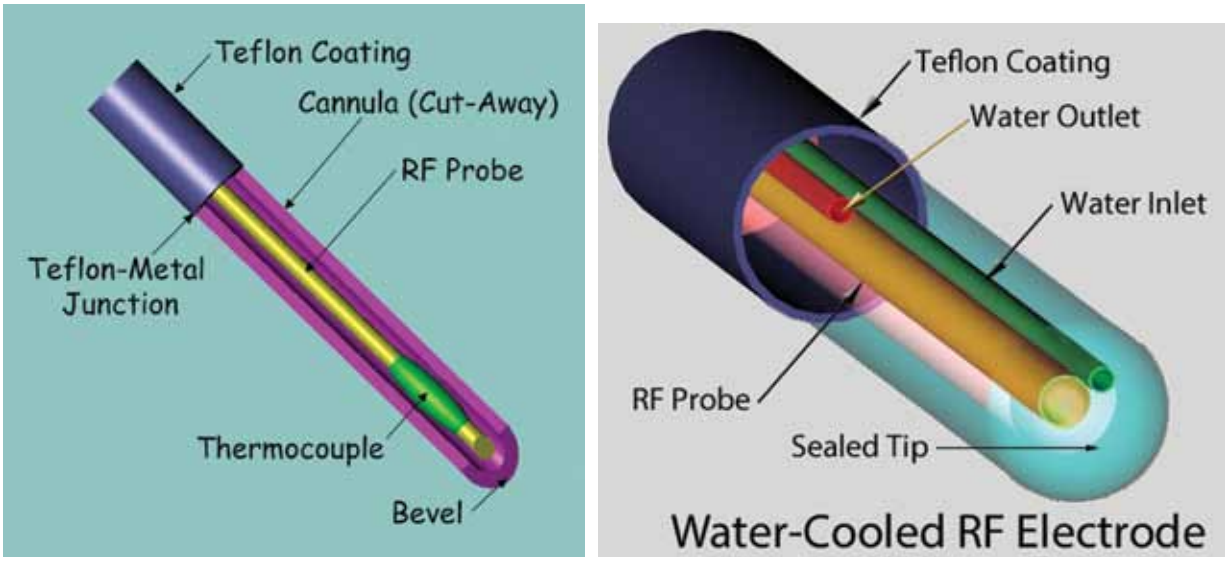

Fig. 1. *RF Electrode Construction. A. demonstrates the components of the active portion of the conventional RF electrode. B. demonstrates the components of a water-cooled RF electrode. Note that the probe is hollow but sealed at the tip. The actual RF conductor containing the thermocouple (yellow) is accompanied by the cool water inlet (green) and outlet (red).*

sue is the critical lesioning temperature (CLT), which varies inversely with the duration of heating (49). The volume of tissue lesioned is the lesion zone (LZ).

The Ground Electrode

A few comments about the ground, or dispersive, electrode are in order. The only requirements for a monopolar ground electrode are that its surface area be large enough that its peak current density (milliamperes/cm^2) is low enough that excessive heating does not occur at the skin-electrode interface. For true monopolar RFA, by definition, the ground electrode is far enough from the ablation electrode that moderate changes in the ground electrode position do not significantly alter the heating pattern of the ablation electrode. These conditions are invariably met in IPM. Since the conventionally placed ground electrode has few effects on the LZ under normal circumstances, it will be viewed simply as a current source/sink, and further discussion will address only the ablation electrode.

The Radiofrequency Signal

The RF signal is an alternating current (AC) radiofrequency waveform, generally between 250 kHz and 1 MHz, applied at an average intensity that maintains the ablation electrode thermocouple at the target temperature. Frequencies are well below the range where microwave phenomena occur. Maximum voltages are manufacturer-specific and range from a few hundred to approximately 1,800 volts peak-to-peak. Instantaneous power output, which ultimately determines electrode thermocouple temperature, is controlled by some combination of modulating the amplitude, shape, and duty cycle of the RF waveform. In an AC system, the ablation and ground electrodes alternate as the anode and cathode. Direct current (DC) is not used for RF ablation systems since the reduction-oxidation (redox) reactions occurring at the electrodes produce undesirable effects and sustained capacitive current flow is not feasible. While direct control over RF generator power output is almost never provided, increasing or decreasing the target temperature has the same net effect on generator output.

Current is carried by electrons in the RF equipment, leads, and probes, but is carried by native ionic species, not electrons, in tissue. Capacitive current, sustainable only in AC systems, is carried by ions moving in response to the RF electromagnetic field (50,51). Capacitive impedance is frequency dependent, decreasing as the RF frequency increases. The capacitance, C, of the typical electrode-tissue interface is in the range of 0.2-1 μF, and the capacitive impedance of the electrode-tissue system at 1 MHz is therefore in the range of $\frac{1}{2\pi fC} \cong$ = 0.2-1Ω, values that would allow a large capacitive current flow (44).

Basic Electrode Heating

The Effects of Different Tissue Types Adjacent to the Electrode

An approach similar to "finite element analysis" is used here to explain RF current flow through the peri-electrode tissues. An "electrode subunit (ES)" is defined as a volume of tissue extending from the electrode surface (electrode-tissue interface [ETI]) to the body-subunit interface (BSI) (Figs. 2 and 3). The BSI is defined as the point in the circuit where moving farther away from the electrode has little additional influence on the LZ, i.e., little additional heating occurs. This will generally be 5-10 mm from the electrode. At this point, it no longer makes sense to include additional tissue in the ES. In the simple situation represented in Fig. 4, muscle, loose areolar/adipose tissue, and bone each represent an electrode subunit because RF current in each tissue flows from the ablation electrode to the BSI under electrically similar conditions which are distinct from the conditions associated with the other 2 electrode subunits composed of different tissue types. Electrode subunits are created until all the types of tissue surrounding the electrode are accounted for, and when all electrode subunits are assembled in a manner analogous to a 3D puzzle, the assembly represents a solid tissue mass surrounding the electrode. The behavior of the electrode can then largely be described as the sum of the behaviors of its subunits.

The main portion of an RF electrode (excluding the ends) in homogeneous egg white *in vitro* could simply be modeled as a cylinder. Conversely, an RF electrode in a complex *in vivo* environment might require 1–2 dozen individual electrode subunits to be accurate.

To illustrate some basic behavior under simple circumstances, assume the ESI and BSI of the overall electrode are represented by cylinders, the BSI obviously having a larger radius than the ESI. The average ratio of the area of the BSI to that of the ETI must be $\frac{r_{BSI}}{r_{ETI}}$, where r_{BSI} and r_{ETI} are the radii of the BSI and the ETI cylinders. While individual electrode subunits may violate this rule, the cumulative averages of the electrode subunits must comply (Figs. 2 and 3). *In vivo*, the aggregate BSI surface need not be a cylinder due to anatomic constraints.

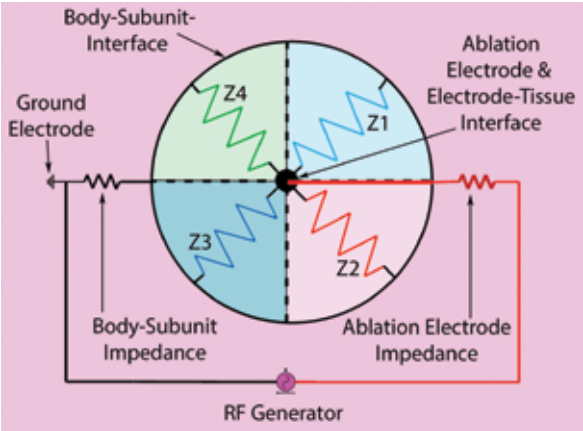

Fig. 2. Tissue disc sectors with variable impedances. This figure is electrically equivalent to Fig. 5, simply re-arranged to show the components as they would appear in an axial section through the electrode and surrounding tissue. Impedances ZxA and ZxB of Fig. 5 have been combined into impedances Zx to simplify the figure. Each quadrant is a separate electrode subunit. The same applied RF voltage will result in different amounts of heat being generated in each quadrant if Z1-Z4 differ, although Z1-Z4 can be identical. Hence, with Z1-Z4 not being identical, target tissue one mm away from the electrode in quadrants 1, 2, 3, and 4 will be heated to different temperatures. The right-hand medial branch sulcus (Fig. 20), viewed posteriorly, could be approximated by quadrants 2, 3, and 4 being largely bone, and quadrant 1 being soft tissue.

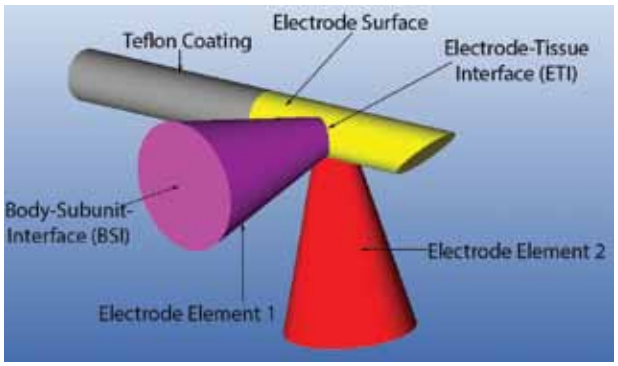

Fig. 3. *Electrode subunit model of RF electrode. An RF electrode is shown with 2 electrode subunits. The electrode subunits consist of the electrode-tissue interface (ETI), the body-subunit interface (BSI), and the tissue in between. The electrode subunits are defined by the preferred route of current between the ETI and the BSI, e.g., the electrode surface is divided into a large number of small sectors, and the current arising from each sector traced to the BSI. Similar tissue pathways are then aggregated into one larger subunit. If the BSI and ETI are considered to exist on concentric cylinders, the average area of the BSI must be larger than the area of the ETI by a factor of* $\frac{r_{BSI}}{r_{ETI}}$. *However, subunits themselves need not be regularly shaped. When all electrode subunits are assembled, the aggregate represents a solid tissue mass surrounding the electrode and will be treated as a cylinder. The behavior of the entire RF electrode is the sum of the behaviors of its electrode subunits.*

This can be summarized by pointing out that all the electrode subunits must add up to a continuous functional electrode structure (electrode plus surrounding tissue), and the outside surface of the structure obviously must have a much larger surface area than the surface area of the metal electrode, i.e., the surface area of the ETI. The above calculations simply quantitate this for a cylindrical structure.

RF generator output is generally in a narrow range once equilibrium at the target temperature is established. A simplified schematic of the system can be represented by 3 impedances in series: the body impedance between the ground electrode and the BSI, electrode subunit impedance, and the ablation electrode impedance. (Figs. 2 and 5, Table 1). The body impedance and the ablation electrode impedance can be adequately represented with simple elements, i.e., no parallel elements. The electrode subunit impedance is a group of parallel impedances, one for each electrode subunit and each subunit consisting of 2 impedance elements in series, one impedance representing the tissue of the electrode subunit excluding the ETI, and the other representing the ETI impedance (including the effects of any injectate). The potential effects of injectate impedances are being brought in to lay the foundation for further discussion of injectate effects in the The Effects of Injectates Prior to RF Lesioning. The total impedance of the overall circuit is high enough that total RF currents through the ablative electrode will rarely average above the milliampere range with the voltages used in lumbar RFR ($(V = IR; I = \frac{V}{R})$) . Figures 2 and 5 show the same circuit, except Fig. 2 has been simplified by combining ZxA and ZxB into one impedance, Zx, and it is visually re-arranged.

The ablation electrode, with an impedance of only a few ohms at most, will never generate significant amounts of heat with the levels of current present in the circuit. The mechanism of electrode heating is analogous to that of a ceramic cup in a microwave oven. An empty ceramic cup does not absorb significant microwave energy, and its temperature rises only minimally when it is microwaved alone. However, if the cup contains water, which absorbs microwave energy very well, the water will be heated and heat conduction will eventually raise the

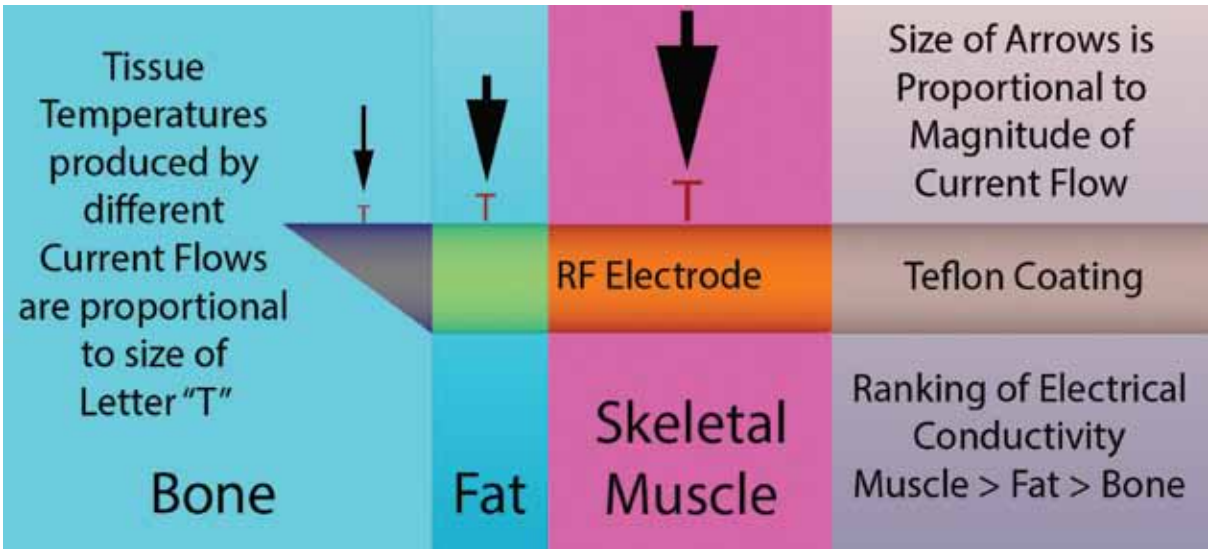

Fig. 4. *Electrode subunit model of RF electrode. RF resistive heating varies with tissue type. Tissues with higher conductivities/lower impedances have higher current flows (represented by the size of the arrows), which if in the proper range, usually result in a greater induced temperature increase, represented by the size of the letter "T." The temperature increase is different for each type of tissue. The electrode does not generate significant heat secondary to its low impedance, but rather is heated by the tissue it is in contact with. The above diagram is a representation of the tissues usually surrounding the RF electrode during lumbar RFR when using perpendicular positioning to lesion the medial branch but also applies to parallel positioning.*

temperature of the ceramic cup to almost that of the contained water.

To summarize, a given electrode subunit produces a characteristic amount of heat for a given RF current, and has a characteristic total heat capacity which determines its temperature rise during RFA. Because of this, the different ES surrounding the electrode are heated to different temperatures unless Zx are identical (Figs. 2-5; Tables 1 and 2).

The Source of Heat Conduction Adjacent to the Electrode

During RFA, each ES is heated by current passage, aka "joule" or "resistive" heating, as shown in Figs. 2–5, as well as conductive heating if adjacent tissues have a higher temperature. Conductive heating is simply thermodynamic redistribution of heat produced by resistive heating. There is no independent heating by thermal conduction, with all conducted heat being originally produced by resistive RF heating (44). Most importantly, if RF heating of tissue does not produce adequate heat, there is no other source. Hence, *in vivo* barriers to current flow must be analyzed critically.

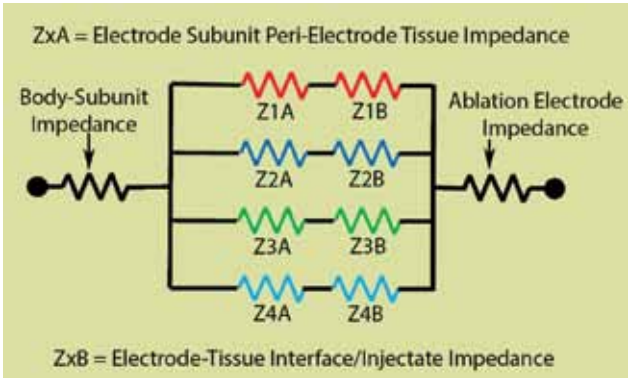

Fig. 5. *Electrode-body impedance model. The "body impedance" represents the impedance of the tissues from the dispersive/ground electrode to the edge of the electrode subunits, and limits maximum current flow, generally to the milliampere range. Impedances ZxA represent the impedance of the electrode subunits excluding the ETI, which is represented by Impedances ZxB, and also includes the effect of any injectate on ETI impedance. The final impedance represents that of the ablation electrode itself. The ETI resistance may be high, and reduce heating (Table 1), and an appropriate injectate can reduce the overall impedance at this point in the circuit.*

Table 1. *Heat and temperature calculations for tissue discs of variable impedance and altered electrode-tissue interface impedance.*

V =	100		Volts	Totals
2	Impedance (Ohms)			
Z1	Z2	Z3	Z4	
25	50	200	1000	
	Actual Current (ma)			
I1	I2	I3	I4	Total I
367	183	46	9	605.5
	Actual Power (Watts)		1 W = 1 J/s	
RI-1	RI-2	RI-3	RI-4	Total P
3.37	1.68	0.42	0.08	5.56
	Total Heat Capacity (J/˚C)			
C_0	C_0	C_0	C_0	
2	2	2	2	
	Temperature Rise (˚C)		1 Sec Heating	
ΔT	ΔT	ΔT	ΔT	
1.683	0.842	0.210	0.042	

(a) ETI impedance = 100 Ω

V =	100		Volts	Totals
2	Impedance (Ohms)			
Z1	Z2	Z3	Z4	
25	50	200	1000	
	Actual Current (ma)			
I1	I2	I3	I4	Total I
526	263	66	13	868.4
	Actual Power (Watts)		1 W = 1 J/s	
RI-1	RI-2	RI-3	RI-4	Total P
6.93	3.46	0.87	0.17	11.43
	Total Heat Capacity (J/˚C)			
C_0	C_0	C_0	C_0	
2	2	2	2	
	Temperature Rise (˚C)		1 Sec Heating	
ΔT	ΔT	ΔT	ΔT	
3.463	1.731	0.433	0.087	

(b) ETI impedance = 50 Ω

Heat and temperature calculations for tissue discs of variable impedance and altered electrode-tissue interface impedance.
These calculations are based on a reasonable voltage being applied between ground and ablative electrodes. The tissues compared in the 4 columns are identical in every way except electrical impedance. The electrode-tissue interface (ETI) impedance is 100 Ωin (a) and 50 Ωin (b). Arbitrary, but reasonable, impedances were assigned to the elements, and the current/power calculations performed for the circuit shown in Fig. 5. Note that as the tissue disc impedance (Z1-Z4) increases, the power dissipation and temperature rise become smaller in each case. At some point, further decreases in Z1-Z4 will be of no value because the body-electrode impedance limits current flow and the power dissipated in each impedance element may actually decrease. Also note that a moderate decrease in the ETI impedance results in roughly a doubling of total power dissipation and temperature rise from (a) to (b). The decrease in ETI impedance resulting from injection of a conducting buffer through the electrode is likely the basis of the increased lesion volume seen after this maneuver.

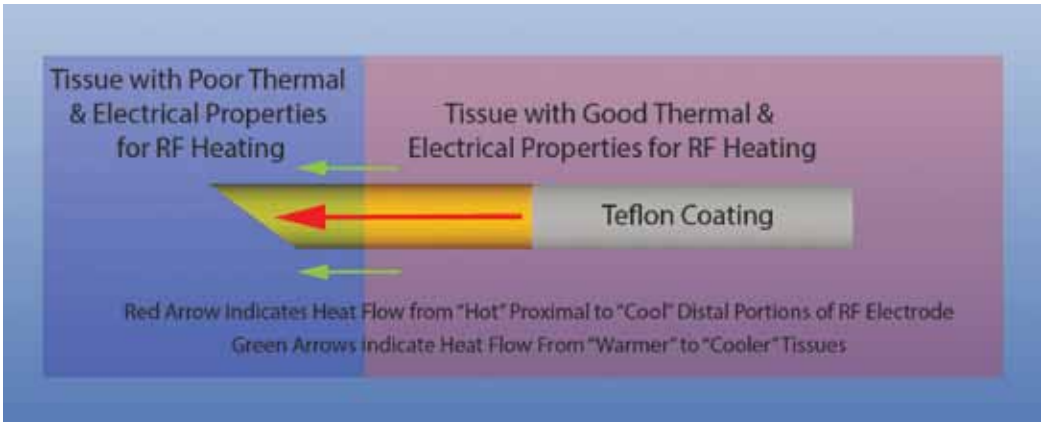

Fig. 6. *The effects of variable electrothermal properties in the tissues surrounding the electrode. Diagram demonstrating how different physical environments for the distal and proximal electrode can create differential heating, proximal greater than distal, with net heat conduction from the proximal electrode to the distal electrode, and from warmer, generally more superficial tissues (reddish) to cooler, deeper tissues (blue). This figure would represent symmetrical sagittal and coronal sections around the electrode in imaging nomenclature.*

Heat Conduction along the Electrode

For metals, the stainless steel alloys used in contemporary RF electrodes are poor heat conductors ($\kappa \approx 15$ W/m-°C), but they are still much better heat conductors than the tissues, most likely even after correcting for the greater cross-sectional area of the tissue (Table 3, Fig. 6). This creates the possibility of temperature differences existing along the length of the electrode (52,53), allowing heat conduction to occur longitudinally along the electrode. This may allow heat conduction along the electrode to play a role in heat redistribution.

Heat Transfer by Convection

Heat may be transported to the target tissue by the process of convection, i.e., heat transfer by the bulk movement of fluids heated near the electrode which then physically move heat to the region of the target tissue. These fluids can be injected buffers, blood, and/or lipid-based tissue components which have been liquefied by RF-induced heat. Convection is a heat transfer mechanism with significant potential to improve RF heating.

360° Current Spread and Factors related to Geometry

Figure 2 demonstrates an axial cross section of arbitrary thickness through an area where 4 electrode subunits, each occupying one quadrant, cover all the tissue in this cross section. For this example, the impedances of Z1-Z4 are specified to be equal. Current can therefore emanate from the electrode against identical impedances from 0°-360° as viewed along the axis of the electrode. The ratio of the area of the BSI to the area of the ETI remains the same. Since the same amount of current flows through the ETI and the BSI, the current density ratio of ETI to the BSI, $\frac{j_{ESI}}{j_{BSI}}$, is $\frac{r_{BSI}}{r_{ETI}}$ i.e., a much higher current density exists at the ETI. Since dissipated heat/power is proportional to j^2, the power dissipated at the ETI relative to the body-subunit interface is $\frac{r_{BSI}^2}{r_{ETI}^2}$.

It can be shown that for 16-22G RF electrodes in this configuration, the majority of the energy, Q, emanating as current from the electrode, is dissipated as heat very rapidly, leaving relatively little energy to be dissipated more than 1–2 millimeters from the electrode.

Moving away from the electrode, heating/energy dissipation decreases as a function of $\frac{1}{r^2}$, such that the intense heating present at the ETI drops off very rapidly with distance.

Simultaneously, the volume of tissue that must be heated, and therefore its total heat capacity, C_t increases as a function of r^2, creating a situation where, moving away from the electrode, Q decreases rapidly as C_t increases rapidly. Figure 7 shows $\Delta T = \frac{Q}{C_t}$ versus r, demonstrating that the calculated increase in tissue temperature diminishes very quickly as distance increases.

The shape of this curve is largely unaffected by electrode type, surrounding tissue type, etc., and is primarily a function of geometry and distance.

Lastly, this decrease in heating with increasing r

Table 2. *Representative conductivities of various tissues at 500 KHz. Representative conductivities of various tissues demonstrate that tissues which are largely considered cellular have much higher conductivities than fat or bone, with blood being the highest (88).*
Saline conductivities (87) are shown for comparison, with 1.0% NaCl, essentially normal saline, having a significantly higher conductivity than the tissues. Conductivities can vary significantly depending on measurement conditions, frequency, and other variables, but the above values are typical and useful for comparison purposes.

Representative Tissue Conductivities	
Tissue Type	Electrical conductivity (S/m)
Normal Liver	0.36
Liver Tumor	0.45
Myocardium	0.54
Fat	0.10
Bone	0.03
Blood	0.70
Vaporized Tissue	~1e-15
NaCl, 0.1%	0.30
NaCl, 0.2%	1.00
NaCl, 0.5%	2.70
NaCl, 1.0%	4.50
NaCl, 5,0%	25.00
NaCl, 36%	45.00

is associated with geometrical changes that increase heat loss to adjacent tissues as a function of r. These phenomena, taken together, dramatically limit the maximum temperature rise that commercial IPM RF systems can produce in locations more than 1–2 mm from the electrode (54-56). This does not mean that the lesion cannot be larger than 4 mm in diameter, since heat can be transferred further than this by conduction and convection, or by restricted channel current spread, discussed below. However, if RF current alone is the mechanism of heating, and 360° spread is dominant, the lesion is going to have a small diameter. Major increases in the RF power input into the electrode shift the curve in Fig. 7 to the right. However, large increases in RF power output produce only small increases in the lesioning distance of the electrode with RF heating alone. Increasing the RF power is always worth doing if the LZ must be enlarged, because this increases the total amount of energy added to the tissues, where it is available for spread by conduction and convection. This is a situation where longer heating times will be useful, shifting the mechanism of heating "distant" tissues from resistive heating to the kinetically slower processes of conduction and convection.

Restricted Channel Current Spread

The previous section was based on current being able to spread out in a 360° radial fashion, thereby being forced to heat a large, expanding volume of tissue. Now consider the case where the majority of current can only exit the region of the electrode by flowing along a channel based on a 30° arc of the total circle, the arc is oriented towards the MB/target tissue , and the same amount of current is flowing as when 360° spread was occurring (Figs. 2 and 8). Also assume that the cross-sectional area and volume of the channel increase much more slowly than they did in the 360° spread example. It can be shown mathematically that, all other things being equal, the theoretical temperature rise in this channel would be dramatically higher and will extend much farther from the electrode than with 360° current spread, greatly extending the effective distance of the electrode.

In most IPM applications, the target tissue will only occupy a small channel/arc, and the remainder of the 360° will be nontarget tissue. This highlights the severe negative effect that 360° spread has in most IPM applications, in that most current is wasted heating nontarget tissues and the effective heating range is relatively short.

Multiple Impedances in Parallel

The only section of our model that qualifies for this type of analysis is the impedance represented by the numerous electrode subunits. The basic laws of current flow in multiple parallel impedances state that the bulk of the current will follow the path of lowest impedance. If there is a significant range in impedance values between parallel elements, the highest impedance element has relatively little impact on total parallel circuit impedance, which is largely determined by the lowest impedance element of the group. In a basic parallel arrangement with simple, passive electrical elements, if parallel elements A, B, and C are passing 60%, 30%, and 10% of the baseline current, respectively, then they will pass 60%, 30%, and 10% of any current increase. In Fig. 4, skeletal muscle, loose areolar/adipose tissue,

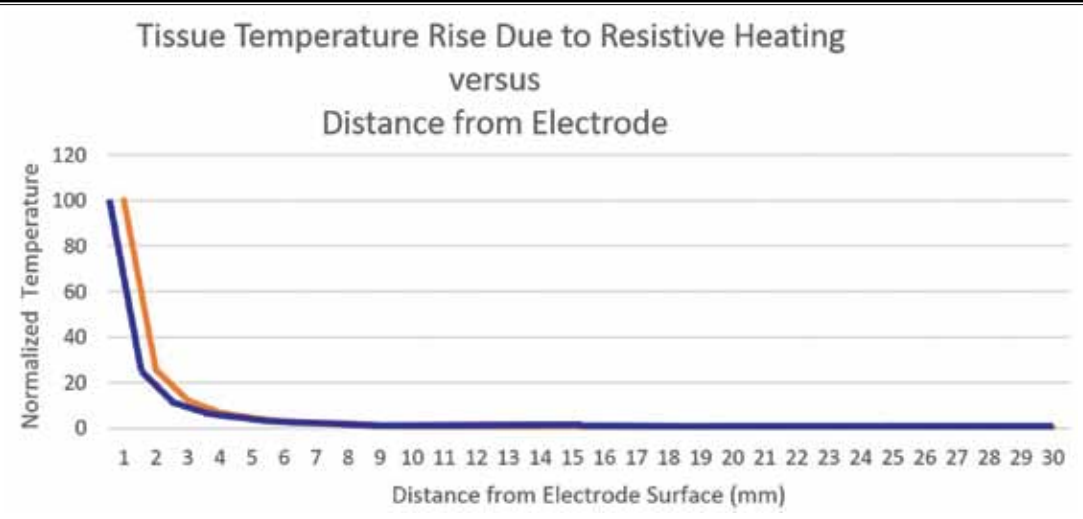

Fig. 7. *Calculated temperature rise produced by RF signal in homogeneous medium as a function of distance from the RF electrode. This curve demonstrates the rapid falloff in RF-induced tissue temperature rise with increasing distance from the catheter, normalized for temperature (see text). The blue curve represents the data obtained with RF power level one. The red curve represents the data obtained after the RF power level has been doubled, and the curve has been "shifted to the right." Note that what is a very substantial increase in RF input power yields a relatively modest increase in the size of the heated zone.*

Fig. 8. "Small" channel current spread.
The complete 360° circle shown in Fig. 2 represents "wide" angle current spread; the current density over the entire 360° arc is at a minimum average value for any given value of current. The above figure demonstrates what occurs when the majority of the total current can only enter/exit the tissues around the electrode from a 30° arc, i.e., "small" angle current spread as shown in the small channel pointing to the right. Ideally, the perimeter of this 30° arc would be in contact with the medial branch. This involves the same amount of current as true 360° current spread but with this current restricted to a small volume of tissue compared to the original circumstances. The heat dissipation and final temperature rise of this small channel will be much higher than the same tissue with 360° current spread. If this could be reliably done under clinical circumstances, the medial branch would be placed in the small channel and would easily reach lesioning temperatures.

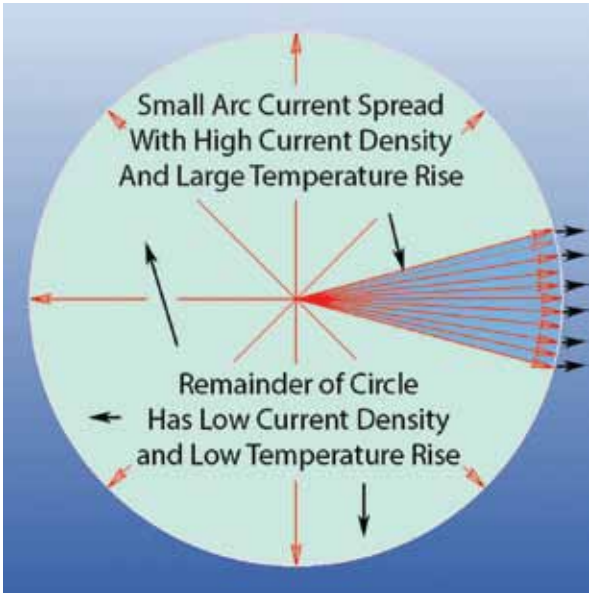

and bone can be thought of as tissues A, B, and C arranged electrically in parallel such that in Figs. 2 and 5 they represent Z1, Z2, and Z3. Z4 will be ignored for the moment. Since skeletal muscle, Z1, has the lowest impedance, it will pass the bulk of the current, i.e., skeletal muscle will "shunt" the current away from bone and loose areolar/adipose tissue. To lesion the medial branch, the current needs to generate heat in the areolar/adipose tissue (Z2) and bone (Z3), but because skeletal muscle (Z1) is shunting the majority of the overall current, Z2 and Z3 see only a small percentage of the total current.

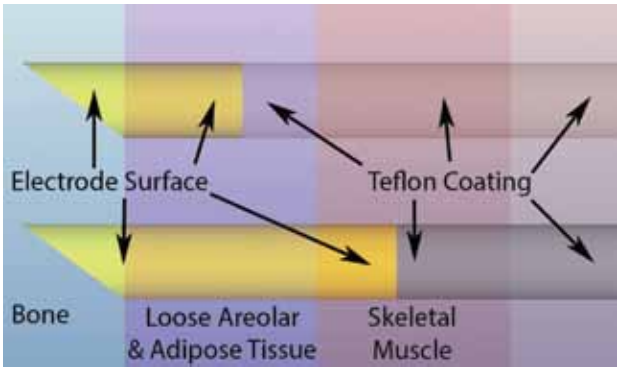

Fig. 9. *Eliminating skeletal muscle contact with electrodes by electrode shortening.*
Two electrodes are shown penetrating skeletal muscle, loose areolar/adipose tissue, and bone. The lower electrode has 10 mm of electrode surface exposed, and a significant portion of the electrode is in contact with skeletal muscle, creating the conditions for shunting of current through skeletal muscle and away from the other tissues.
This skeletal muscle is present in both parallel and perpendicular electrode positioning.
The upper electrode is identical with the exception of only having 5 mm of electrode surface exposed. This removes electrical contact between the electrode and skeletal muscle as well as eliminating the shunting described above.

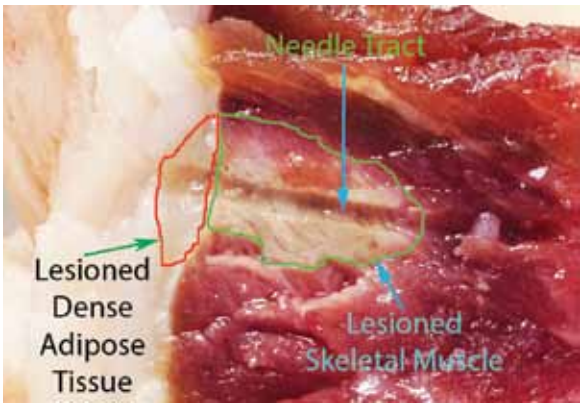

Fig. 10. Tip heating in an environment involving hemispherical current flow.
A beef skeletal muscle with a thick overlying layer of dense adipose tissue is shown after a 90s/80°C RF heating cycle with the 10 mm RF electrode perpendicular to the fat-muscle interface. Approximately 3 mm of the electrode is penetrating fat and the proximal 7 mm is in skeletal muscle. Inserting more of the electrode into the adipose tissue invariably results in an RF generator fault, either by high impedance or an inadequate rate of temperature rise, both the result of the electrical properties of the adipose tissue. The skeletal muscle is well lesioned, and while there is obvious damage to the adipose tissue, it is limited. The temperature probe is located in the extreme end of the electrode, positioned in the adipose tissue, and this is almost certainly the coolest portion of the electrode. In this case, the shunting of current by skeletal muscle prevents full power from heating the adipose tissue, which represents the tissue in contact with the MB. The safety settings of the RF generator also limit power application to adipose tissue alone since these conditions create a fault condition.
Some heat involved in lesioning the adipose tissue was produced by current flowing in the tissue, some heat was undoubtedly conducted from muscle to adipose tissue through the electrode, and some heat was conducted directly from heated muscle to adipose tissue, illustrating the complexity of how target tissue can be heated, and also illustrating how power dissipated in nontarget tissue can be conducted into target tissue. The skeletal muscle lesioned here, albeit impressive, likely does not contribute significantly to the success of the RF procedure.

Because of this, little current in this example is going to generate heat around the MB (51), but rather is going to heat nontarget tissue, i.e., skeletal muscle. It is difficult to work around this problem, with the exception that Z1 can be largely eliminated by using a 5 mm electrode instead of a 10 mm electrode, effectively covering the electrode section within skeletal muscle with Teflon, leaving only Z2 and Z3 exposed to metal (Fig. 9).

Figure 10 was obtained with a perpendicular orientation at the junction between dense adipose tissue and skeletal muscle. The impedance of dense adipose tissue is low enough that if more than approximately 50% of the length of a 10 mm electrode is embedded in the adipose tissue, the RF generator will fault, either from excessive impedance or an insufficient rate of rise of electrode temperature during initial heating. A 5 mm electrode completely embedded in the adipose tissue suffers the same fate. The original intent of this figure was to show the equivalent of Fig. 9 *ex vivo*, but the commercial IPM RF generator would not function with a 5 mm electrode in the adipose tissue due to the above issues.

The impedance of the loose areolar/adipose tissue overlying the MB is such that a 5 mm electrode with typical parallel positioning over the medial branch target zone (MBTZ) will usually not fault the system. A 5 mm electrode in this position has only Z2 and Z3 to heat. A well-positioned 5 mm RF electrode will likely be more effective in lesioning the MB than a 10 mm electrode, due to the elimination of Z1 and its associated shunting.

With shunting by Z1 eliminated, 100% of any current increases obtained by raising the target tempera-

ture will pass through Z2 and Z3, all likely heating the MB.

In most situations involving the application of RFA, extensive contact of the electrode with skeletal muscle or other highly conductive tissue is likely deleterious unless the associated shunting produces useful heat.

The Time and Temperature used for RF Exposure

For the moment, it is assumed that maximum destruction of the MB is the goal of RFA. Examining only the heating component (Appendix A), this goal is best met by applying the maximum RF power to the target tissue until the target temperature is achieved and then for whatever additional time is necessary to achieve the desired results. The de facto standard of 90 seconds of heating with a target temperature of 80°C was informally adopted in the 1970s–1980s, but these values were largely transposed from *in vitro* experiments, e.g., with egg white, not from clinical studies (Fig. 11). The rationale was based on the fact that the size of the egg white coagulum did not increase much between 60 sec and 90 sec. However, there is only a loose relationship between this and whether the MB is adequately heated. The rate of RF power input may slow around 90 seconds, but in almost all systems, longer exposure times invariably produce some increase in lesion size (24).

The source of 80°C is less clear, but is likely related to this being the highest temperature that older RF generators and electrodes could consistently attain without regular generator faults.

Manipulation of time and temperature parameters is underutilized in devising more effective RF heating protocols, and needs to be re-evaluated. It is highly likely that there will be a benefit associated with increased RF exposure times, and this question cannot be answered with *in vitro* experiments.

Note that optimal time and temperature will depend on multiple variables and there will likely not be a single "best" time and temperature to cover all conditions.

Disruption of Electrode-Tissue Interface Function

The major limitation of maximum RF power output is disruption of conductivity at the electrode-tissue interface (3,52). If tissue at the electrode-tissue interface desiccates, boils, or chars, it becomes a high impedance insulator. These phenomena underlie most of the gradual or sudden increases in impedance that can occur during RFA, and will usually result in an RF generator fault.

The temperature at which these events occur is known as the "electrode interface disruption temperature" (EIDT), generally near 100°C. The purpose of water-cooled RFA systems is to keep the electrode-tissue interface below the EIDT while higher RF power is applied to the electrode.

Historical Data from Protein Coagulation Systems

For many years, IPM physicians were using egg white coagulation experiments for studying RF electrode behavior. To put older *in vitro* experiments on RFA electrodes in context, some discussion of "protein coagulation systems (PCS)," usually egg white or skeletal muscle, is necessary. Despite their shortcomings, important conclusions have been reached with PCS. PCS are based on nearly homogeneous substances that produce an easily detectable and generally irreversible visual change when heated to a threshold temperature, analogous to the CLT *in vivo*. The protein in egg white coagulates in the range of 63°–66°C, and an egg white PCS provides information regarding when and where coagulation conditions are produced.

PCS results should be interpreted carefully, as they give a binary result, i.e., an area either coagulates or it does not. One electrode system may produce significant visible coagulation in egg white when the coagulation temperature is barely exceeded, e.g., 67°C, whereas another system may produce no coagulation when the maximum temperature is just below the coagulation temperature, e.g., 62°C. The PCS results imply a large difference between the 2 systems, but the difference is actually small, and both systems exceed the CLT. Likewise, an electrode system may produce a wide range of temperatures, but if they all exceed the coagulation temperature, they will appear identical. PCS should rarely be used for comparative studies.

Figure 11 demonstrates the coagula obtained at various points in an egg white PCS for 90 seconds at 80°C. Almost none of the published experiments considered how free convection modifies the heating patterns observed *in vitro*. Egg white is a fluid gel that becomes less dense when heated. When a conventional RF electrode is oriented tip down, heated egg white flows upwards along the electrode shaft, transferring heat by convection to the upper portions of the electrode and the egg white surrounding it. Under these circumstances, coagulation in egg white starts at the

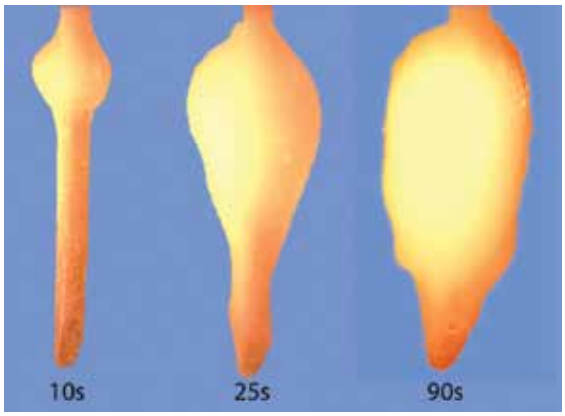

Fig. 11. *In vitro coagulum versus time with conventional RF electrode.*
Egg white coagula resulting from a heating cycle with a conventional RF electrode at a target temperature of 80°C. At 10 seconds, the protein surrounding the Teflon-metal junction is coagulating, with minimal distal coagulation. At 25 seconds, the typical "conical" coagulum shape has formed. At 90 seconds, the final coagulum has formed, with the bulk proximally and relatively little over the tip.

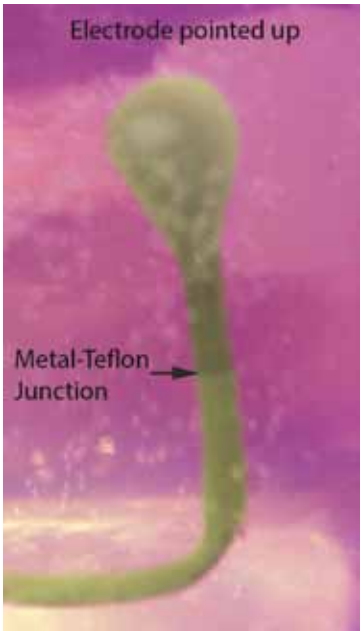

Fig. 12. *The effects of convection heating on coagulation patterns. Coagulum produced when the electrode is bent into a "J" shape so that the tip of the electrode is pointed up. In this case, free convection provides additional heating to the tip of the electrode as opposed to the metal-Teflon junction as occurs when the tip is pointed down. The pattern seen here is the reverse of the pattern obtained with the tip pointed down, indicating that convection produces the asymmetry, not some intrinsic property of the RF system or electrode.*

metal-Teflon coating junction (Fig. 11, 10 seconds), and thereafter the coagulum increases in diameter while coagulation on the bare electrode surface travels distally towards the tip (Fig. 11, 25 seconds). Eventually, the coagulum slows, proceeding distally and increasing in diameter proximally; the last phase involves a slight to moderate increase in diameter of the distal coagulum (Fig. 11, 90 seconds) (56,57). Only rarely is there significant coagulum over the tip of the electrode (56).

Reversing the orientation of the electrode, e.g., bending it into a "J" shape such that the tip now points up instead of down, a coagulum of similar shape and orientation is obtained. However, the new coagulum is 180° reversed with respect to the electrode tip/axis, as the tip is now covered with coagulum whereas the metal-Teflon junction is bare (Fig. 12). The explanation for this is the addition of convection heating to the other heating of the upper electrode, creating the most intense heating around the uppermost electrode, regardless of which portion of the electrode is "uppermost." During lumbar RFA, convection of this magnitude is unlikely to occur, and as a general rule, no conically shaped LZ would be predicted *in vivo*. This is an excellent example of how seemingly minor alterations in electrode positioning and/or environment can produce large differences in the LZ, and also an example of the pitfalls that can be encountered examining electrode behavior *in vitro* or *ex vivo*. One should interpret all older literature using PCS cautiously, and only in the context of what the study is attempting to demonstrate. Solid PCS systems, without convection, e.g., agar or skeletal muscle, are preferable, all other things being equal. This is also an example of how convection, when it does occur, can be a major positive or negative influence on the results of RFR.

Electrical Modeling of the Ablation Electrode

It is helpful to define conceptual zones around the electrode for use in mathematical modeling and for explanation purposes. These models are largely for *in vitro* use, and to provide a vocabulary for discussing electrode behavior. (Figs. 13 and 14):

Zone 1: The interior of the cannula, consisting primarily of the RF probe and retained liquid. It generates no significant heat but is where the probe tem-

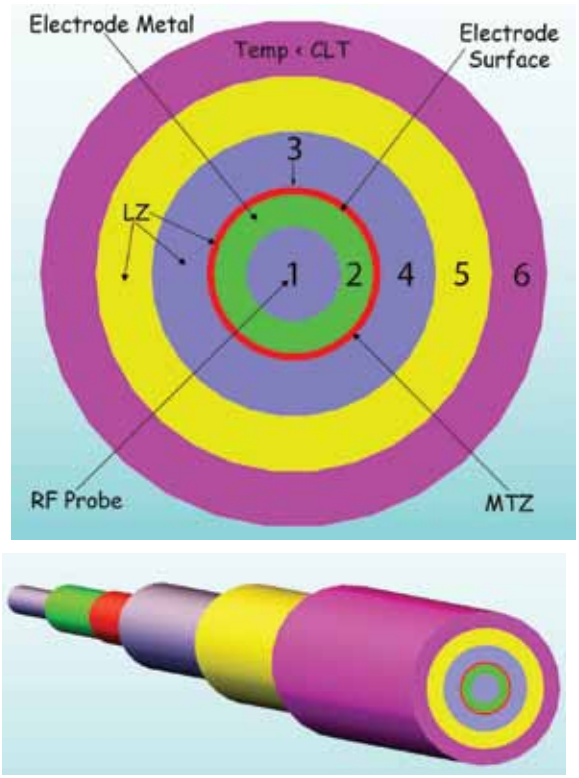

Fig. 13. *Six heating zones of the conventional RF electrode. See text for zone definitions. Zone 2 is the metal of the cannula, Zone 3 is the MTZ, also the location of the EIDT. The temperatures in Zones 3, 4 and 5 produce severe thermal damage, defining the lesion zone. Zones 1-3 can be physically measured, whereas the dimensions of Zones 4-6 are determined by heat flow equations, while the boundary between Zones 5 and 6 can be determined empirically, in that it demarcates the LZ.*
Note that the MTZ, Zone 3, is immediately adjacent to the electrode proper, but belongs to the tissue, not the electrode.

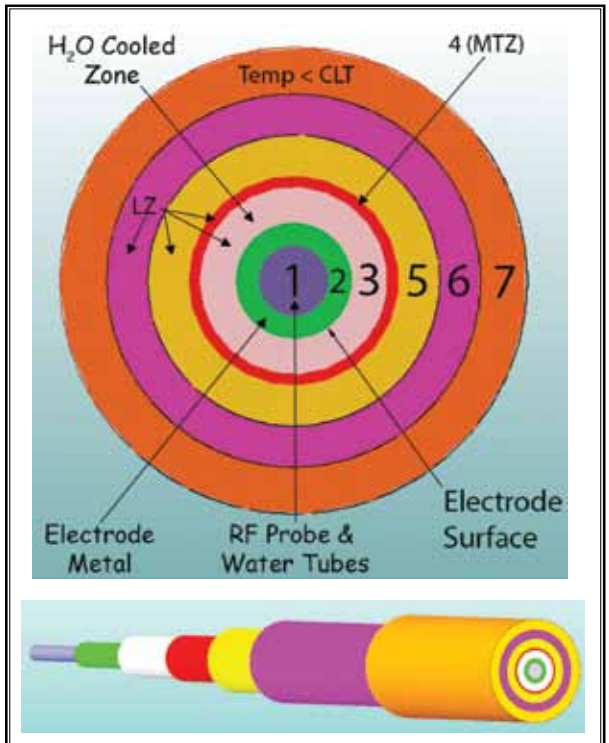

Fig. 14. *Seven heating zones of water-cooled RF electrode. The outer electrode surface, the location of the MTZ of conventional RF electrodes is located at the junction of Zones 2 and 3 (see text, Fig. 13). As a result of water cooling, an additional new zone, Zone 3, is created and the MTZ is now displaced radially to Zone 4, analogous to a conventional RF electrode whose diameter is equal to that of the "new" Zone 3. The water cooling makes the inner portion of Zone 3 significantly cooler than the outer portion of Zone 3.*

perature is measured. The temperature rise here is produced by heat flowing inward.

Zone 2: The metal of the electrode. Current flow occurs here, but there is little heat generation.

Zone 3: The junction between the electrode and the peri-electrode tissues where electrochemical reactions occur. This layer is only a few nanometers thick. It is associated with high impedance, a large voltage gradient, maximum current density (⌈), and substantial heat production relative to Zones 4 and 5. Zone 3 is the maximum temperature zone (MTZ) and location of the EIDT of the conventional RF system, and belongs to the tissues, not the electrode.

Zone 4: The tissue immediately outside of Zone 3, which is heated by resistive heating plus heat conducted from Zone 3.

Zone 5: The tissue peripheral to Zone 4 which is heated by resistive $Z * J^2$ heating plus heat conducted from Zone 4. By definition, all tissue in Zone 5 is heated to or above the CLT, with the boundary between Zone 5 and Zone 6 being where temperatures drop below the CLT. Zone 4 is heated primarily by RF resistive heating while heat conduction plays a much larger role in Zone 5, the source of the heat being Zone 4. Conductive heating does occur in Zone 4 and resistive heating occurs in Zone 5, but the predominant mode of heating reverses from Zone 4 to Zone 5.

Zone 6: The tissue peripheral to Zone 5, outside the LZ,

where some heating and damage occurs, but it is reversible.

Figure 14 shows an analogous figure modified to apply to the water-cooled RF electrode. This is similar to that outlined above, but there is one additional zone, Zone 3, which is a new zone created by water cooling. If zones are indexed to the MTZ, the water-cooled Zone 4 is equivalent to the conventional Zone 3, with the water-cooled Zone 3 being a new, previously nonexistent zone (Figs. 13 and 14). The inner boundary of the water-cooled Zone 3 is at the target temperature, but moving away from the electrode, RF heating gradually overcomes cooling, and the temperature increases until the MTZ is reached in Zone 4. The outer boundary of the water-cooled Zone 3 is therefore essentially at the MTZ temperature. The outer limit of the water-cooled LZ is now between Zone 6 and Zone 7. The conventional Zones 3–6 are equivalent to the water-cooled Zones 4–7.

The Critical Lesioning Temperature

The minimum temperature and time required to irreversibly lesion the MB is not known with certainty due to the lack of a suitable test system. It is known that heating for 90 seconds at 80°C with a conventional RF electrode can produce a clinically excellent rhizotomy, but these are probably not optimal parameters. There is not a unique CLT, but rather a CLT versus time curve, whereas when the temperature increases, the required lesioning time decreases, and vice versa (32,39,49). A 90 second heating time is assumed in the following discussion.

In general, most mammalian cells are eventually irreversibly damaged at a temperature of 46°C–49°C. However, in MB ablation, neuronal axon, the vascular supply, and associated axonal cells (e.g., Schwann cells) are heated, not the neuronal cell body. It is unknown if these entities have the same susceptibility to heat as do cardiac myocytes and hepatocytes, where most data on RFA-induced cell death has been collected. Based on the data available, it is unlikely that the CLT for lumbar RFA exceeds 55°C, and may be significantly lower (58,59).

The CLT is important in 2 situations since it is usually exceeded in most of the LZ: at the boundary between conventional Zones 5 and 6, and the water-cooled Zones 6 and 7, where the temperature by definition is the CLT; anything that increases heat transfer to this region increases the size of the lesion. This may be amenable to manipulation by using longer heating times and higher electrode temperatures. At the other extreme, when using contemporary water-cooled RF electrodes, overly aggressive cooling might bring the electrode surface too close to the CLT to be 100% effective heating tissue very close to the electrode, particularly if heat loss in that area is prominent.

The Diameter of the RF Electrode

The current density, j, at the electrode-tissue interface, is the highest j in the electrode system since this area has the minimum surface area through which the total RF current must pass. This is where tissue will boil/char first. Hence, to avoid exceeding the EIDT, either I at the ETI must be kept under the threshold value, or some type of cooling must be applied to the electrode.

Using a cylinder based model, the surface area (SA) of the electrode increases linearly as a function of electrode diameter, i.e., $SA = 2\pi r * l$, where I = the length of the electrode. If a small diameter RF electrode in a given situation is replaced by an electrode with twice the diameter, the surface area doubles, as does the maximum total electrode current for a given I. Therefore, all other things being equal, there will be 4 times the heating produced with the larger electrode since heating is proportional to j^2. This is a primary reason why larger electrodes produce larger lesions (56,57). Figure 15 shows an axial view of a 16G electrode and a 20G electrode. The thickness of the concentric rings around the electrodes represent the tissue temperature rise obtained at maximum j. As is obvious, the 16G electrode is far more effective.

As shown by the phantom medial branches, when the nerve and electrode are parallel, the large electrode can be significantly out of position, and still heat the nerve, whereas the smaller electrode allows for little error in positioning.

Lastly, there is an element of tissue compression produced when the electrode displaces the soft tissue while it is being positioned, e.g., blood and extracellular fluids are forced out, making the tissue thinner and eliminating the need to heat the expelled fluids. The degree of tissue compression will be greater for the large electrode. The larger electrode will likely be effective because it is heating tissue that is more highly compressed, and there will be more cell parenchyma exposed to the CLT. This would be the same effect produced by applying hand pressure to the RF electrode during the rhizotomy, forcing it against the MB.

If there are problems with excessively high electrode impedance or inadequate rates of heating, an electrode with a higher surface area may solve the problem.

Lastly, blood flow in target tissue interferes with lesioning via convective heat removal, and tissue compression by the electrode may attenuate blood flow in

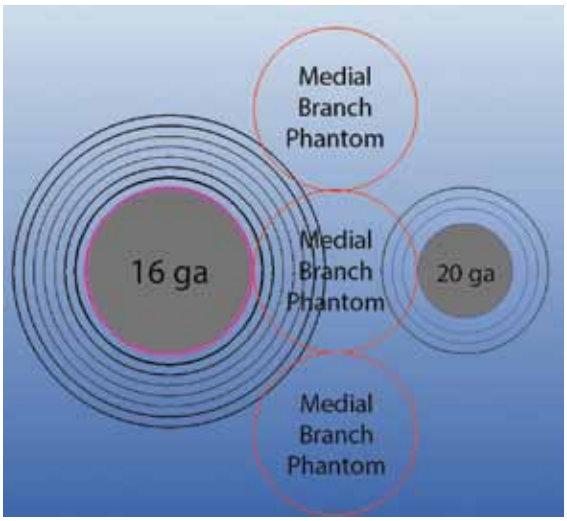

Fig. 15. *Tissue temperature rise versus electrode size. The lesioning diameter around a 16G electrode (diameter = 1.6 mm) compared to a 20G electrode (diameter = 0.9 mm). The outer ring on each diagram represents identical temperature increases for identical conditions to provide a basis for comparison. The rings demonstrate temperature rise, not cell damage, since cell damage cannot be calculated mathematically. This is a diagram showing "360° current spread" and it can be seen that the 16G electrode is much more effective than the 20G electrode. The current chosen for both electrodes is the maximum current that can be passed without exceeding the EIDT; j is similar for both electrodes. The medial branch phantoms show that there is a great deal of error permitted in positioning the 16G gauge electrode while still damaging the MB, whereas little error is allowed with the 20G electrode before the MB escapes thermal damage.*

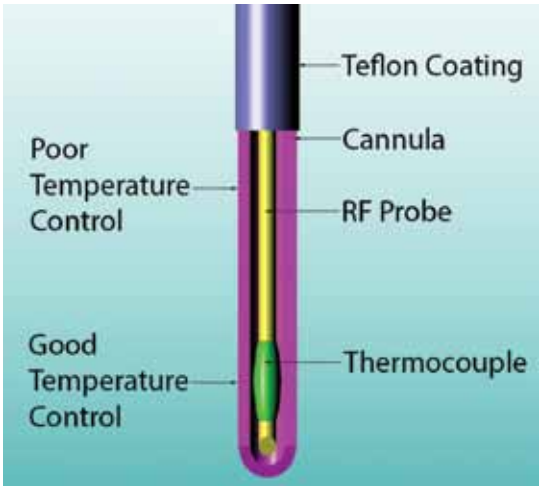

Fig. 16. *Temperature sensor displacement. Conventional RF electrode having a distal thermocouple. Tissue temperatures near the electrode tip are close to the thermocouple temperature, whereas temperatures near the proximal electrode may differ significantly. The temperature of the surface of the water-cooled electrode is usually similar throughout.*

peri-electrode tissues, reducing heat loss and resulting in a larger LZ (60,61).

The Effect of Tissue Thermal Conductivity on Lesion Size

The outer zones of the LZ, Zones 5 and 6 for conventional RF electrodes, and Zones 6 and 7 for water-cooled RF electrodes, are influenced by the thermal conductivity of the surrounding tissue. If the surrounding tissue has a relatively low thermal conductivity, i.e., is a relative insulator, heat flow out of the outer zones will be decreased, and more energy will be retained in the LZ. As a result, LZ temperatures will be higher, but the LZ volume will be smaller, because of restricted heat loss peripherally. This can be beneficial when lesioning tissue adjacent to poorly conducting tissue such as bone. However, tissues with significant thermal insulating properties almost always generate less resistive heat (62) because they also have low electrical conductivity, making it difficult to predict whether the heat gain of the outer LZ is increased by the insulation effect or decreased by the poor resistive heating (63). This is a situation where longer heating times may compensate for the lower heat production of tissues such as adipose tissue and bone (64). The amount of tissue that must be heated is also important, in that a perfectly placed RF electrode may have very little soft tissue to heat, in which case, decreased heat production may not be an issue.

Temperature Errors related to Thermocouple Location

The temperature of different portions of the RF electrode surface varies significantly, with the most reliable information being that the thermocouple temperature is close to the target temperature. The thermocouple does not perfectly measure the temperature of the tissues surrounding the tip, let alone the temperature of the proximal electrode (Fig. 16). The RF generator maintains the thermocouple/distal electrode near the target temperature, and the proximal electrode and its environment are dependent variables, assuming whatever temperature results from the conditions set to maintain the thermocouple temperature as well as the nature of the peri-electrode tissues. In lumbar RFA, the proximal

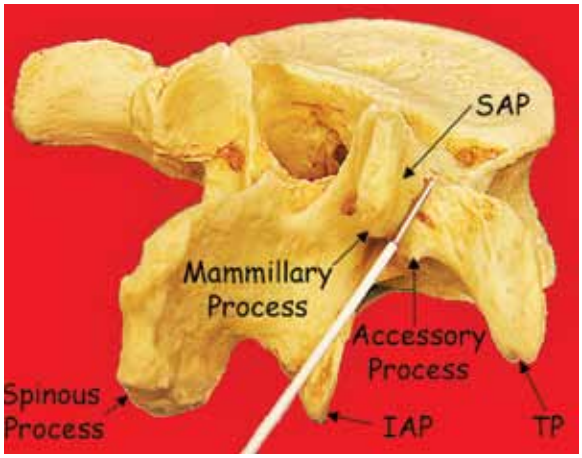

Fig. 17. *Positioning the RF electrode over the MBTZ. Positioning of the RF electrode as recommended by Bogduk. The medial branch runs under the mamillo-accessory ligament posteriorly, which defines the location of the nerve there. These posterior bony landmarks can be difficult to identify radiographically. While the accessory process is well seen here, the mammillary process is not well visualized, although its position can usually be inferred from the "waist" of the SAP in a lateral radiograph. The "target region" of the MB correlates well with an imaginary "belt" around this waist. The position of the accessory process must frequently be estimated. The most reliable bony landmark for the posterior position of the MB in a lateral radiograph is the caudal edge of the base of the SAP. Anteriorly, bony landmarks are less discrete, but viewed with caudad angulation, the main portions of the SAP and TP form a rounded junction with each other, and bisection of the arc of this junction is an excellent approximation of where the MB is positioned anteriorly. The active portion of the electrode should cover a zone that is slightly larger than the middle one-half of the "waist" of the SAP in a lateral view. The RF electrode should be as parallel to the surface of the MBS as possible.*

electrode is expected to be hotter than the distal electrode due to the types of tissue located around the electrode (Figs. 2–5, 8 and 10). Regardless of the approach in the lumbar region, the electrode generally must pass through muscle, connective tissue, and onto bone, in that order. The patterns just reviewed could be reversed in the anatomic environment of other procedures, but for lumbar RFR, the proximal electrode is expected to be hotter and the EIDT will almost certainly occur on the proximal electrode first.

Positioning the RF electrode for Lumbar RFA

Accumulated data (12,56,65-72) support the view that positioning of the ablation electrode parallel to the MB produces more effective lesioning than does nonparallel positioning. As reviewed, the conventional RF electrode heats well along the shaft, but probably not at the tip. This was recognized by Bogduk some 30 years ago, and he subsequently also delineated the target region of the MB where it is most susceptible to thermal damage, the MBTZ, located in approximately the middle 50% of the base of the superior articular process (SAP) (8,9,11,73-78). His recognition of the MBTZ may have been one of his more important contributions to the area, even if the degree of its importance was not specifically recognized at the time. The specifics of this position are outlined visually and radiographically in Figs. 17–19 per Bogduk's criteria. The details of electrode positioning are given in the figure legends.

Implicit in this localization is that a 5 mm electrode would be located between the MB/bone and the epimysium of the overlying muscle, a well insulated compartment where heat loss should be low, the heat capacity of the tissues low, and heating should be very effective (Fig. 20).

Figure 20a shows a cross-section of the medial branch sulcus with placement of the electrode next to the medial branch. Figure 20b shows a suboptimally placed electrode with soft tissue in between the electrode and the medial branch. In actual practice, the same electrode could produce both pictures if the base of the SAP were convex, in that perfect placement is present where the electrode is tangent to bone, but the bone curves away from the electrode in front of and behind the tangent point (Fig. 21). In addition to the positioning criteria given above, bending the electrode to match the curvature of the underlying bone should be attempted where feasible. This maneuver is usually easier with a 5 mm electrode than a 10 mm electrode.

The Effects of Poorly Conductive Tissue on RFA Heating Patterns

Returning to the microwave oven analogy, consider a watertight ceramic hemicylinder where the ablation electrode is positioned parallel to the center axis of the hemicylinder, 2 mm–3 mm away from the flat surface, and outside the chamber (Fig. 22). The medium surrounding the electrode and covering the exterior of the hemicylinder is heated poorly by the microwave signal and also has poor thermal conductivity, similar to bone or connective tissue. The water in the hemicylinder is the only material heated well. The electrode and sur-

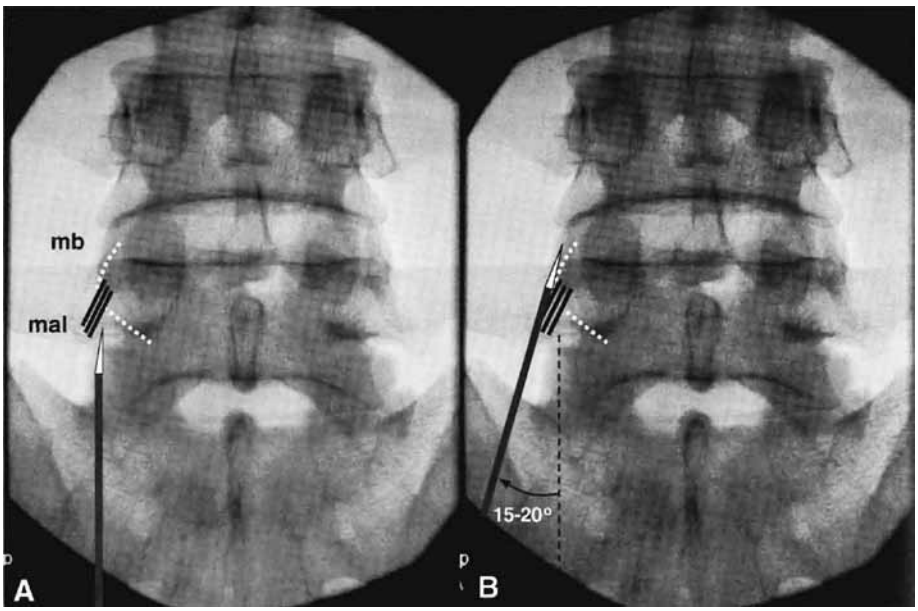

Fig. 18. *Anteroposterior radiographs of proper RF electrode placement.*
These anteroposterior radiographs of a Lumbar RFR at L4-L5 demonstrate proper electrode placement in (B), along with improper placement in (A) where there is insufficient lateral angulation. This is probably the most common mistake made in this projection since in (A), the electrode will impinge on the posterior SAP/Mammillary process, and placement adjacent to the MB will be prevented since the electrode will be displaced too far laterally by bone. (mb) = medial branch; (mal) = mamillo-accessory ligament.

Bogduk, N. (ed). ISIS Practice Guidelines: Spinal Diagnostic & Treatment Procedures. International Spine Intervention Society, San Rafael, CA, 2004, pp 201, 202.

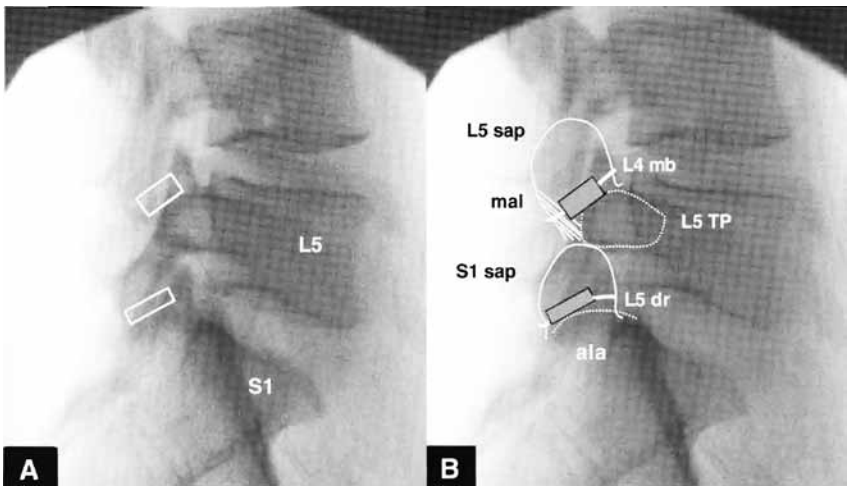

Fig. 19. *Lateral radiograph of proper electrode placement at L4-L5 and L5-S1.*
Lateral radiograph (A) demonstrating the location of the target region of the medial branches, and hence the desired electrode location during RFR. Radiograph (B) with superimposed drawings of the target regions of the medial branches at these levels. (TP) = transverse process; (dr) = dorsal root of L5; (sap) = superior articular process.

Bogduk, N. (ed). ISIS Practice Guidelines: Spinal Diagnostic & Treatment Procedures. International Spine Intervention Society, San Rafael, CA, 2004, pp 201, 202.

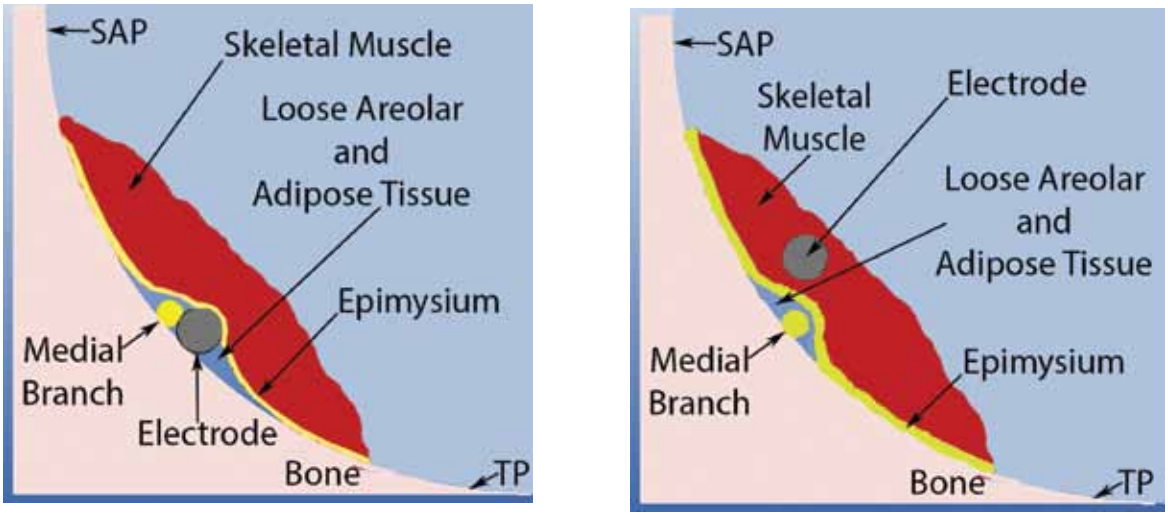

Fig. 20. *Electrode placement in the medial branch sulcus.*
(a) The lumbar RF electrode placed by the criteria of Bogduk. The medial branch is shown lying on bone, with the RF electrode in this same compartment and no insulating connective tissue between the medial branch and the electrode. The nerve and electrode lie on bone, and are overlaid with the loose areolar/adipose tissue and skeletal muscle/epimysium present over the medial branch sulcus. The loose areolar/adipose tissue and epimysium are relative insulators. Heat loss is lowered, and the medial branch, as well as its supplying vasculature, should reach higher temperatures under these circumstances.
(b) Shows a sub-optimally positioned RF electrode with approximately 1-2 mm of loose areolar/adipose tissue, epimysium, and skeletal muscle between the electrode and the medial branch.
See Fig. 26 for an ex vivo picture similar to what is represented above.

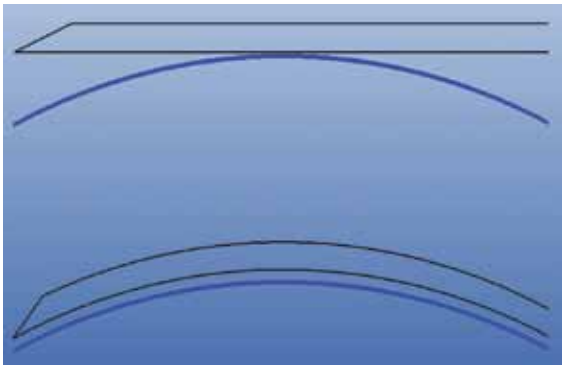

Fig. 21. *Compensating for curvature of the SAP and/or TP. When the SAP and TP under the MB is fairly straight, no modification of the electrode may be necessary (Fig. 17). However, the bony surface is also frequently curved. The bony surface is represented by the heavy blue line in both the upper and lower figures. In the upper figure, the electrode has been left straight, and the large gap between electrode and bone can be seen to widen on either side of the tangent point. In the lower figure, the electrode has been bent to match the curvature of the SAP, producing good proximity of the electrode and nerve along the entire length of the electrode. When possible, the electrode should be modified to increase contact.*

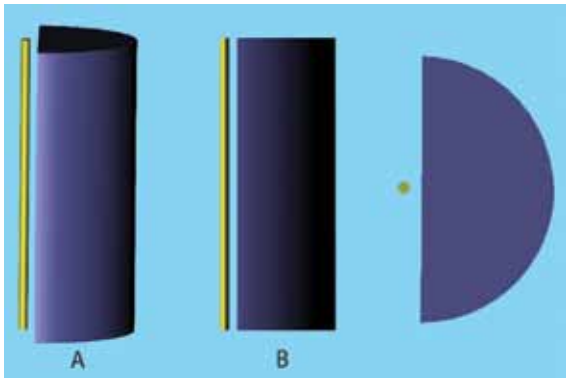

Fig. 22. *Hemi-cylindrical heating by the RF signal. Diagrams of a ceramic hemi-cylinder, filled with liquid (dark blue), and heated in a microwave oven. The yellow rod represents the RF ablation electrode. A) Side view from slightly above; B) Side view; C) Top view. Only the dark blue liquid is heated by microwaving. The light blue medium to the left of, and surrounding, the electrode represents a material with minimal thermoelectric conductivity and has little temperature rise when microwaved. A situation analogous to this can occur during lumbar rhizotomy when the RF electrode is heating target tissue near bone and is surrounded by tissues with poor thermoelectric properties such as fat. Much less heating occurs outside the dark blue fluid.*

Table 2. *Representative conductivities of various tissues at 500 KHz.*
Representative conductivities of various tissues demonstrate that tissues which are largely considered cellular have much higher conductivities than fat or bone, with blood being the highest (88). Saline conductivities (87) are shown for comparison, with 1.0% NaCl, essentially normal saline, having a significantly higher conductivity than the tissues. Conductivities can vary significantly depending on measurement conditions, frequency, and other variables, but the above values are typical and useful for comparison purposes.

Representative Tissue Conductivities	
Tissue Type	**Electrical Conductivity (S/m)**
Normal Liver	0.36
Liver Tumor	0.45
Myocardium	0.54
Fat	0.10
Bone	0.03
Blood	0.70
Vaporized Tissue	~1e-15
NaCl, 0.1%	0.30
NaCl, 0.2%	1.00
NaCl, 0.5%	2.70
NaCl, 1.0%	4.50
NaCl, 5.0%	25.00
NaCl, 36%	45.00

rounding area are heated by heat conducted/radiated from the heated water and ceramic surfaces and by relatively inefficient microwave heating. Therefore, a structure a few millimeters away from the ceramic surfaces receives little heat relative to a structure within the heating zone. Changing the configuration of objects heated from a cylinder to a hemicylinder largely spares tissues in the unheated half of the hemicylinder.

The example given is analogous to a 180° current spread, but any angle could be chosen to represent a specific *in vivo* situation. Lumbar RF is probably best represented by a current spread angle of approximately 100° (Figs. 2 and 20), where bone occupying roughly quadrants II, III, and IV represents the 260° of the circle that is not well heated. The conductive tissue in the 100° arc (Quadrant I) shunts the current away from bone.

"Good heating" and "poor heating" are not absolute, e.g., there is always heat produced in the "cool" regions, just less than in the "hot" regions. The bone is heated to some degree as well.

Table 2 shows that the electrical conductivity of

Table 3. *Representative thermal conductivities of various tissues.*
Selected representative thermal conductivities of various tissues. Column (a) (116), (b) (117). The values for muscle and adipose tissue have a narrow range, with muscle being significantly higher than adipose tissue, but the values for bone can vary from roughly 0.2 W/(m-°C) to 0.5 W/(m-°C) depending on the ratio of cancellous to cortical bone, blood supply, etc. It is not known exactly what the thermal conductivity of the bone underlying the medial branch actually is (117-126). These types of measurements are technically difficult to do in vivo.

Tissue	**K(W/(m-deg C))**	
	a	**b**
Cancellous Bone	0.29	0.4
Brain	0.55	0.54
Skeletal Muscle	0.51	0.5
Adipose Tissue	0.19	0.25
Skin	0.43	0.42

bone and fat are generally in the range of 10%–30% that of tissues such as liver and muscle, while thermal conductivity of bone and fat are in the range of 40% that of more highly water-based tissues (49,79-88) (Table 3).

It should be possible to use these phenomena to force adequate heat production near the MB, while the insulating effect retains the heat in the area. If conditions are proper, the possibility of excellent heating immediately adjacent to the well-heated elements exists because of conducted heat trapped by the insulating effect of connective tissue and bone.

Summary of Basic Electrode Heating

There are a large number of variables affecting RF electrode heating. These can be divided into intrinsic properties, e.g., conductivity, heat capacity, tissue heterogeneity, etc., and geometric properties, e.g., 360° current spread versus small channel current spread. The limitations imposed by the EIDT are yet one additional constraint. The net effect of these variables can result in an infinite number of electrode heating patterns, one of which is shown in Fig. 23.

When 360° current spread and parallel impedances in nontarget tissue are prominent, i.e., the tissue around the medial branch is not within or in contact with the low impedance element of the group, increasing total RF power alone is an inefficient way to increase RF heating and conduction/convection must be maximized.

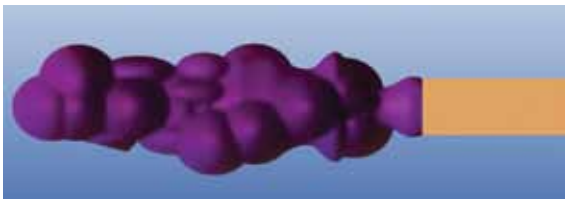

Fig. 23. *An example of one possible real-life in vivo 3-dimensional lesion zone produced by inhomogeneous current flow.*
This very irregular structure is produced by combining the asymmetry of heating in the longitudinal and radial dimensions and is totally dependent on the tissues surrounding the electrode during heating. We are defining the surface of the purple object as being analogous to the boundary between Zone 5 and Zone 6. An almost infinite number of these 3-dimensional isotherms could be produced from an electrode with relatively minor electrode movement. The only time this isotherm will even remotely resemble a symmetrical cylinder is in electrically and thermally homogeneous medium in vitro with convection eliminated, illustrating the difficulties of trying to reduce lesion zones to simple tables. Again, these tables obtained in vitro do provide useful information, but it must be carefully extrapolated to the in vivo situation.

Using a commercial RF generator and placing a major portion of an electrode into tissue with low electrical and thermal conductivity, e.g., dense adipose tissue, will either result in a generator fault related to excessive impedance or an inadequate rate of temperature rise, and if no fault occurs, the target temperature will be maintained with relatively little power due to the insulating effect of the adipose tissue.

Placing the electrode in a tissue with high electrical and thermal conductivity, e.g., skeletal muscle, will almost never result in a generator fault, and maintaining the target tissue will require large amounts of power due to the high rate of power dissipation and poor thermal insulating properties of skeletal muscle. However, most of this heat is wasted because it usually does not contribute to heating the MB.

Water-Cooled RF Ablation

Water-cooled RFA is intended to prevent the electrode-tissue interface from reaching the EIDT, a simple task theoretically, but water-cooled systems as currently manufactured for IPM have some unique behaviors that complicate their use. With water-cooled RFA, water is circulated through the electrode interior, and the electrode, thermocouple, and peri-electrode tissues are cooled from the center outward (Fig. 14). Perhaps the most common target temperature for water-cooled RF ablation in IPM that has emerged is 60°C. The characteristics of and temperature gradient within the "new" Zone 3 of a water-cooled RF electrode are discussed in the Electrical Modeling of the Ablation Electrode section. If we compare "identical" conventional and water-cooled electrodes in infinite, electrically homogeneous media, the conventional RF electrode surface with a target tissue of 80°C is hotter than the 60°C surface of the water-cooled RF electrode surface. The decreasing temperature associated with moving away from the conventional RF electrode eventually equals the rising temperature of the equidistant tissues surrounding the comparable water-cooled RF electrode. This is the "crossover distance" in Fig. 24, past which point the water-cooled RF electrode produces higher temperatures and is a more effective lesioning tool (88). In large tissue volumes, or PCS, the water-cooled RF electrode will produce a much larger LZ, and will produce a significantly larger lesion over the tip relative to the conventional RF electrode.

So long as the water-cooling prevents the electrode-tissue interface from reaching the EIDT, the temperature of the cooling water has little effect on lesion size, suggesting that there is no reason to cool any more aggressively than necessary to avoid the EIDT (38).

Water cooling changes the way that heat is added to the tissues. Heat is removed from the electrode-tissue interface where the RF heating easily produces the CLT and frequently the EIDT as well, but is added to tissues further from the electrode via increased RF signal intensity, thereby lesioning tissues which could not be adequately heated at the previous RF output levels (88).

In some cases, there will be no difference in effectiveness between the 2 electrode types, because the target tissue is inside the crossover distance, and a 60°C electrode temperature for the water-cooled RF electrode will be adequate to lesion the target tissue. However, in the case of lumbar RFR, where the medial branch lies on bone, inside the crossover distance, covered with connective tissue, in a setting of hemispherical heating (Fig. 22), the conventional RF electrode is likely superior. Accurate placement of a water-cooled RF electrode for lumbar RFR with parallel positioning immediately adjacent to the MB heats the electrode surface to only 60°C, as opposed to the 80°C present with conventional RFR, and this 60°C assumes that there is no heat loss from the area, which is never the

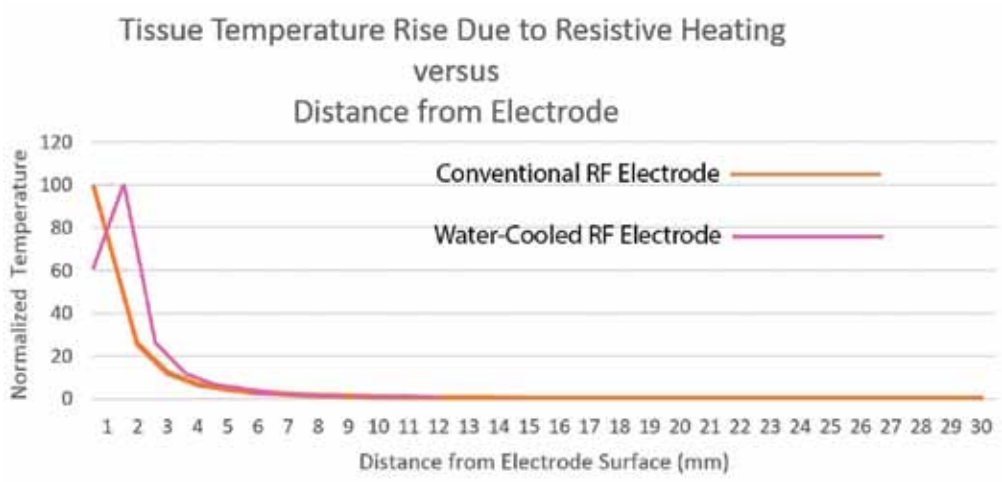

Fig. 24. *Heating patterns of conventional and water-cooled RF electrodes.*
The conventional RF electrode has its highest temperature at the electrode surface with steadily decreasing temperatures moving away from the electrode. In contrast, the water-cooled RF electrode has its highest temperature approximately 1-2 mm away from the electrode surface, the exact distance depending on the intensity of the RF signal and the aggressiveness of water cooling. One important consequence of this behavior is that temperatures immediately adjacent to the conventional RF electrode are higher than those immediately adjacent to the water-cooled RF electrode based on the commonly used 80°C target temperature for the conventional electrode and the 60°C target temperature for the water-cooled electrode.

case. If heat loss is large enough, the CLT may not be reached. With lumbar RFR, it will be difficult to predict *in vivo* how the water-cooled RF electrode is going to behave at distances less than the crossover distance.

The water-cooled RF electrode may have better tip coverage by the criteria of *in vitro* PCS, but conditions are so much different in clinical lumbar RFR that rigid verification is needed to confirm that the electrode is capable of creating a clinically useful tip lesion *in vivo*. The water-cooled electrode is subject to the same problems as the conventional RF electrode, e.g., hemicylindrical heating, etc. Since the actual tip of the water-cooled RF electrode itself is probably cooler than the tip of the conventional RF electrode, and the perpendicular orientation suggested for lumbar RFA is in an environment of hemicylindrical heating, one has to question how much tip heating is occurring in this environment *in vivo*, even with the water-cooled RF electrode.

There may be circumstances where the larger LZ around the water-cooled electrode might place nontarget tissues at risk, when that risk might be negligible using a conventional RF electrode. The operator must recognize this and adapt accordingly.

Water-cooled RFA is one solution to the MTZ/EIDT problem. The target temperature set in the RF generator is still the temperature of the temperature-sensing element in the electrode probe, but now the thermocouple does little more than verify that the system is working properly to maintain the target temperature. An RF generator target temperature of 60°C with water-cooled RF may produce an MTZ temperature of 98°C. The target temperature of conventional RFA provides some approximate information on the tissue temperatures around the distal electrode, but the target temperature of water-cooled RFA provides little information other than the temperature of the thermocouple.

With conventional RFA, the overall process can be monitored to some degree by observing the absolute values and rate of change of temperature, power output, and impedance. With water-cooled RFA, the cooling process masks almost all of the operator's ability to monitor the process because of the large power losses to cooling.

Water-cooled electrodes are only beneficial when the EIDT is the main limiting factor on RF output, and the soft tissue environment around the electrode meets the criteria previously outlined. The anatomic environment of many IPM pain procedures, e.g., adjacent to bone, are likely situations where the increased heating associated with water cooling probably primarily affects nontarget tissue. If the EIDT is not the limiting fac-

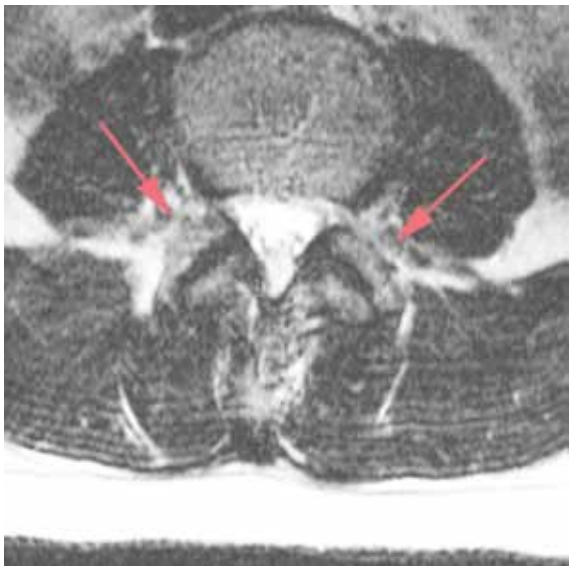

Fig. 25. The environment of the medial branch. The medial branch sulcus (MBS) contains significant amounts of areolar tissue with lesser amounts of interspersed adipose tissue and other connective tissue. The target region of the medial branch is rarely in contact with muscle. The above T2-weighted MRI images show adipose and connective tissue as white and muscle as dark. The arrows point to the region of the MBS, lateral to the SAP, which is largely filled with tissue that is bright on T2 images. There is asymmetry of the posterior elements in the above images, but it is difficult to find patients with perfectly symmetrical facet joints whose MRI images are perfectly symmetrical. The author has examined many lumbar spine MRI studies, including custom studies, e.g., oblique to the axial plane, etc., and has seen no significant variations from this tissue pattern overlying the MBS.

tor in electrode heating, e.g., where RF current flow is limited not by the EIDT, but by tissue impedance, water cooling will obviously be superfluous.

As water cooling is currently applied, oncological and cardiac applications are much better suited to benefit from its use than IPM applications. Water-cooled RF is relatively well understood in PCS *in vitro*, but there is probably much to learn about its behavior *in vivo*.

Clinical Considerations Relevant to Lumbar RFA

The Soft Tissue Environment of the Medial Branch

The electrical and thermal properties of the soft tissue surrounding the MB are critical determinants of the amount of RF heat produced in that area. The MB lies in the MB sulcus with a "wall" of bone formed by the lateral surface of the SAP and a "floor" of bone formed by the upper surface of the transverse process (12,65,66,72,89,90). Figures 20 and 25 illustrate the soft tissue environment of the MB in cross-section. Note that the loose areolar/adipose tissue volume is variable and generally not high. The amount shown should be taken only as an approximation. Electrically, other important tissues are the epimysium and associated skeletal muscle.

The soft tissue immediately overlying the MB is primarily connective tissue, e.g., loose areolar tissue interspersed with adipose tissue (66,91). Overlying the medial branch sulcus, but generally not directly in contact with the MB, is the portion of the longissimus thoracis pars lumborum (LTPL) arising from the accessory process of the vertebra above the level being lesioned, and possibly other portions of the LTPL (66,90,92). The major connective tissue structure is the deep epimysial complex of the LTPL overlying the MB. These tissues (Fig. 26), have a low electrical and thermal conductivity compared to skeletal muscle (Tables 2 and 3). The importance of insulating tissue such as epimysium is illustrated by the fact that in cardiac epicardial ablation, a layer of epidural fat as thin as 2 mm will largely protect the underlying epicardium from RF damage (32,93). Similar tissue with low conductivity is shown insulating the medial branch in Figs. 20, 25, and 26.

Positioning of the RF Electrode by Motor/Sensory Stimulation

Motor/sensory stimulation is frequently used to position the RF electrode. However, this technique has major limitations used alone and has never really been validated. The 18G-22G RF electrode is probably most commonly used in the 10 mm length. As a probe for self-positioning the RF electrode, the dimensions of the electrode are huge, primarily its length, and there is no reason to expect precision. A 5 mm electrode might be more accurate, but no data are available for this situation.

It can be shown that the 10 Hz–50 Hz localizing stimulus for motor/sensory stimulation may not reflect how RF current is going to heat the area (94). A motor/sensory stimulation response only indicates that the stimulating electrode is capable of depolarizing a nerve, since it is usually impossible to distinguish between stimulating a sub-branch of the MB versus stimulating the MB itself. However, there should be few, if

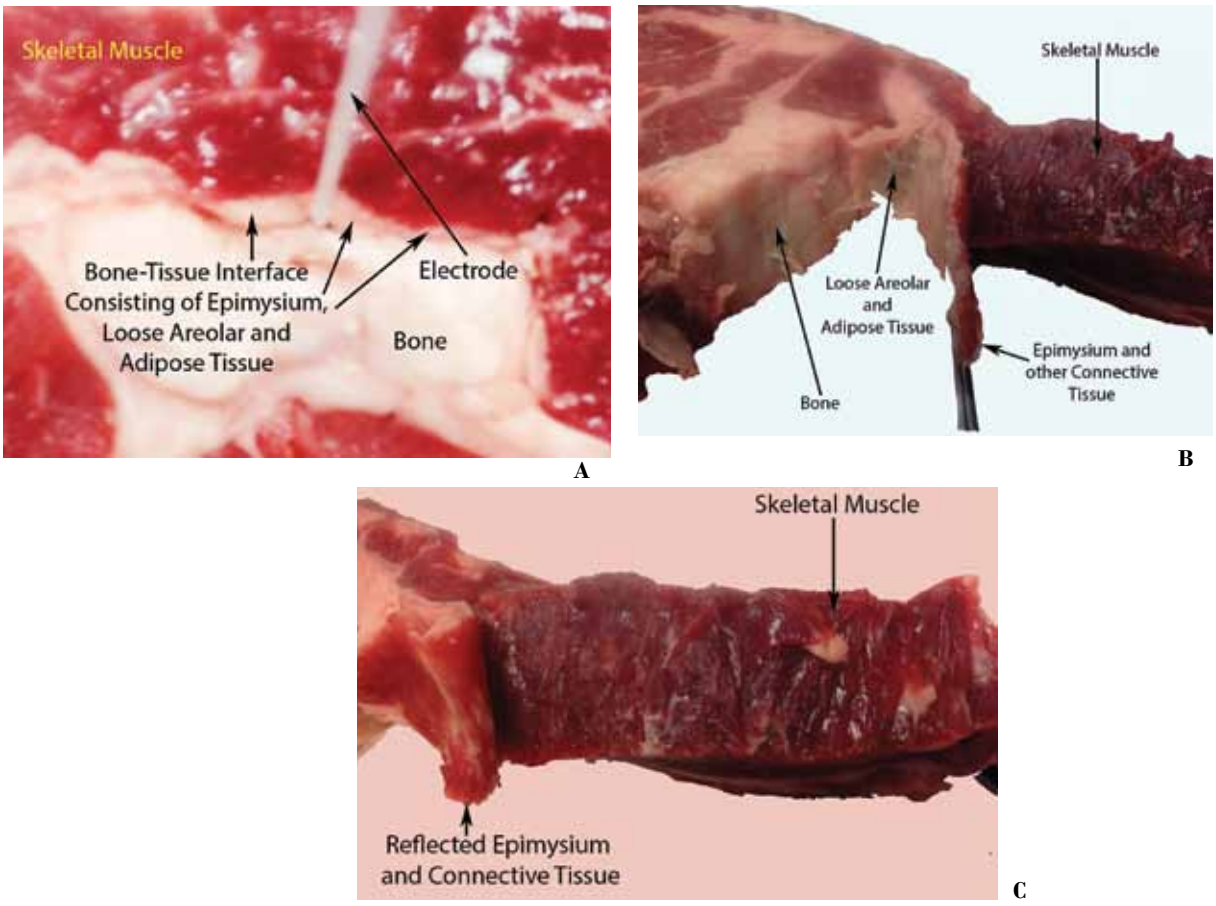

Fig. 26.RF electrode behavior in an environment similar to that of lumbar RFR.
(a) Shows a cross section of beef with a central core of bone and an RF electrode inserted between the bone and the connective tissue/epimysium of the overlying skeletal muscle. This is similar to the anatomic arrangement with lumbar RFR. One RF heating cycle of 90 seconds with a target temperature of 80°C was carried out with the electrode completely enveloped in the bone-muscle interface, as is probably the ideal positioning for RFR. The electrode had no direct contact with skeletal muscle, epimysium always being positioned between muscle and the electrode. Whereas a "normal" RF cycle in a large section of skeletal muscle would require 8-10 W to maintain the target temperature, only 1-2 W was required to maintain the target temperature in this configuration. (b) Shows the cross-sectional view after RF heating with the bone exposed, the epimysial layer reflected, and the deep face of the muscle exposed. While heat damage can be seen on the bone with direct observation, it is difficult to see in the photographs, although it lies under the "bone" arrow. Very little heat damage is observed on the epimysial flap, primarily due to its white color and physical resilience, and virtually no heat damage is seen on the skeletal muscle itself (c) where coagulation should be easily seen. This is an example where the characteristics of the RF generator do not force much current through the impedance of the overall electrode complex, and it illustrates how a very thin layer of electrically nonconductive tissue can largely protect adjacent tissue under the right circumstances.

any, sub-branches of the MB proximal to the region of the mamillo-accessory ligament, although the intermediate and lateral branches must be considered.

With parallel positioning, a 10 mm electrode may stimulate the MB almost anywhere along its course from the anterior aspect of the MBTZ (Fig. 17) to somewhat posterior to the region of the mamillo-accessory ligament, especially in smaller patients.

Electrical stimulation can have a role in localization. There is relatively little uncertainty in electrode placement other than in the cephalo-caudal axis. If an insulated electrode with an extremely small active tip

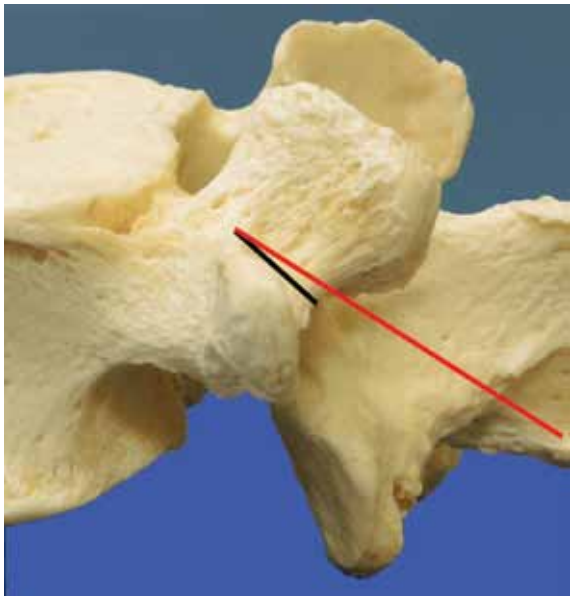

Fig. 27. *Cephalocaudal localization of the medial branch with focused stimulation.*
The black line represents the medial branch extending from the anterior aspect of the MBTZ to the point where the nerve runs under the mamillo-accessory ligament. It is not a shadow of the red line, which represents a small stimulating electrode. If the medial branch is approached laterally with the stimulating electrode (long red line) and there is no contact between the tip of the electrode and the lateral (intermediate) branches, then any evoked motor response obtained must come from stimulation of the MB. Leaving the stimulating electrode in place as a marker, the ablation electrode (not shown) can be positioned in the anteroposterior axis radiographically, viewing the problem in polar coordinates with the tip of the stimulating electrode being the origin, and the caudad and lateral angulation being Ø and θ, determined radiographically prior to electrical stimulation (see text and Figs. 17-19).

is inserted from a superolateral position and directed toward the anticipated location of the MB at the anterior aspect of the MBTZ, the cephalo-caudal position of the MB can be localized by stimulation (Figs. 17–19 and 27). This allows the operator to use this point as the origin to work in polar coordinates. The localization electrode should be small enough that it can be placed accurately without anesthesia. This will be referred to as "focused" stimulation hereafter.

The cephalocaudal and mediolateral angles, Ø and θ, should be determined early in the procedure by radiographic criterion. The cephalocaudal angle of insertion can be determined either by projecting the sagittal angle of the medial branch by the method of Bogduk (Fig. 19), or using focused stimulation at 2 locations to define a line, the latter method being considerably more time consuming, but probably slightly more accurate. The mediolateral angle from the midline sagittal plane can be determined radiographically (Fig. 18), and with the fluoroscope set to these angles, the ablation electrode is directed precisely towards the tip of the focused stimulation electrode with the goal of touching the tips of the 2 electrodes together and then advancing the RF electrode approximately 2 mm further to ensure good heating in the extreme anterior portion of the MBTZ (Fig. 27). Electrode placement is probably easier in polar coordinates where the tip of the electrode is located at (r, Ø, θ), Ø is the caudal angle from the axial plane, and θ is the lateral angle from the midline sagittal plane. This is probably the most precise technique for ablation electrode positioning, with pure anatomic positioning under fluoroscopic guidance being the next most accurate. Relying on electrical stimulation with the RF electrode alone for positioning probably carries an unacceptably high false positive rate, i.e., stimulation indicates that the electrode is close to the MB and in a good position for heating when it is not.

Motor stimulation, using focused stimulation, may also assist localization in situations involving a severely deformed spine to prevent inappropriate positioning of the RF electrode.

Using the thin, focused stimulation electrode for localization without anesthesia, and then placing the RF electrode with anesthesia during insertion, makes the size of the RF electrode irrelevant from a pain standpoint.

Of existing studies, one study failed to demonstrate any improvement in clinical outcome comparing combined motor/sensory stimulation (95) to motor stimulation alone (96); another study found that motor and sensory stimulation had no effect on clinical outcome (97).

Laceration of the Medial Branch

Early in the history of RFA, some open surgical neurectomies of the MB were performed, but very little is known about the long-term clinical results of these procedures. The rationale for using RF ablation instead of mechanical transection has always been stated anecdotally to be the avoidance of painful neuromas, and at least partial preservation of multifidus function. This makes sense from an *a priori* standpoint but has not been verified in terms of controlled studies. Anatomi-

cally, it would be fairly easy to lacerate the MB with the RF ablation electrode, but it should also be easy to avoid. It is tempting to postulate that MB laceration might play a role in a percentage of those rhizotomies associated with atypical and excessive postprocedure pain.

"Natural" Experiments Reflecting RF Electrode Behavior

The phenomenon illustrated in Figs. 11 and 12 are examples of electrode behavior where alterations of seemingly minor variables result in profound changes in the RF heating patterns. Another situation warranting discussion is a natural experiment that occurs during bipolar lumbar RFA procedures using 2 identical electrodes.

Most RF generators in bipolar mode modulate the RF power input by maintaining the hotter electrode of the bipolar pair at the target temperature. The cooler electrode then assumes whatever temperature is produced by the current passing through it, which is identical to the current passing through the "hot" electrode. With constant current through the cooler electrode, its temperature is purely dependent on its tissue environment. Relatively minor position changes of the cooler electrode can result in temperature changes of 30°C or more (personal observation). While electrode positions can be adjusted so that temperatures of both electrodes are similar, it usually requires numerous adjustments in the cool electrode position and is usually time-consuming. This "experiment" proves that dramatic changes in electrode heat production can be achieved by small changes in the electrode position/soft-tissue environment.

The Effects of Injectates Prior to RF Lesioning

The immediate environment of the electrode is the critical area for current flow, and one of the approaches receiving recent attention is injecting a conducting buffer through the RF electrode just prior to lesioning. While studied primarily *in vitro*, these injectates do appear to enlarge lesion size (97-102), and probably operate in several ways.

First, the ETI is an area of potential high impedance, deleteriously limiting current flow. As discussed in Figs. 2 and 5 and Table 1, the electrical impedance of the injectate can be considered to be a series element of the ETI impedance, and as such, the ETI and injectate impedance should be at their minimum level. Tables 1(a) and 1(b) show that a modest reduction in this impedance produces significant increases in electrode power dissipation and tissue heating.

The injectate likely lowers the electrode subunit impedance by several mechanisms. The injectate replaces some of the tissue in contact with the electrode, and via diffusion or replacement presumably lowers the impedance of the ETI and the actual tissue in contact with the electrode.

Lastly, the injectate may help distribute heat to the target tissue by convection/conduction.

However, the injectate has the potential to be a negative factor, in that it can steer RF current away from target tissue. Where heating is produced in target tissue, it is beneficial. Where heating is diverted away from the target tissue, it is useless. Additionally, the injectate must be heated. It would be predicted that very minimal volumes should be sufficient to produce the maximum electrical effect. The more injectate placed in the tissues, the higher the heat capacity of the region, and the lower the temperature rise for a given amount of added heat unless correspondingly more heat is generated. Low and medium viscosity buffers usually migrate away from the electrode *in vivo* in well under a minute under radiographic observation, and much of the increase in lesion size is lost if the RF heating is delayed even 60 seconds after the injection of buffer. This suggests that a very viscous buffer that retains its general physical shape/continuity for the duration of heating would be most effective.

This approach can only be carried so far, in that the ETI impedance will approach a minimum, at which point there can be no more current increases. When this is combined with conditions where the injectate volume is at a minimum and no useless shunting of current occurs, no additional benefit can be obtained. The literature would indicate that the increase in lesion volume *in vitro* attributable to this maneuver is in the range of 10%–40%. If *in vivo*, conditions are such that this additional heat is delivered to target tissue which previously received almost no heat; the modest increase in overall power delivery may be much more important than it appears, and conversely, if the *in vivo* increase goes to nontarget tissues, it may be meaningless. The increase in lesion volume in *in vitro* PCS tells us nothing about these latter factors, and may be deceiving because injectate *in vitro* is retained in the lesion zone in almost all protocols.

Discussion

There may need to be significant changes in how lumbar RFR is performed. There are numerous conditions and events that can cause RF heating to fail or be severely attenuated. Foremost in developing best practices for this procedure is avoiding these pitfalls. Good RF heating and medial branch lesioning are the rewards for understanding how the process functions, attention to detail, and meticulous attention to electrode positioning.

RF electrode contact with tissues having high electrical and thermal conductivity (skeletal muscle) should likely be avoided unless it is known that the heat produced by shunting heats the target tissue. The medial branch and the tissues immediately surrounding it do not have high thermal or electrical conductivity. With lumbar RFR, the proximal portion of the commonly used 10 mm electrode without a doubt shunts significant current through skeletal muscle (LTPL) in all but the largest patients. Unless the RF heating produced in the LTPL by the proximal electrode produces damage to sensory branches innervating painful structures, this is wasted heat. There is little evidence that relevant nerve damage would occur by this mechanism, but the possibility has not been excluded either. If this type of heating is important in producing the clinical results of lumbar RFR, the entire process of the mechanism of lumbar RFR needs to be re-thought. However, at least for innervation of the facet joints at the lesioning level, there are numerous arguments against this mechanism being effective, primarily due to the relative size of the SAP and the size/location of the posterior LZ. On anatomic grounds, the descending branch innervating the facet joint caudal to the lesioning level is probably not vulnerable. These theoretical possibilities obviously need either validation or invalidation.

Hence the general recommendations that RF electrode contact with skeletal muscle be avoided, in that successful lesioning of the MB in the MBTZ most likely makes any thermal events occurring more posteriorly essentially moot. While the optimal electrode length to avoid electrical skeletal muscle contact has not been determined, it is probably less than 8 mm, and probably closer to 5 mm (Fig. 7), which is a typical measurement of the width of the MBTZ.

One feature of a properly positioned 5 mm electrode is that typically, this configuration dissipates only 1–3 W of power during RF heating, compared to the 5–9 W frequently seen with 10 mm electrodes. This data is consistent with Fig. 9, in that if the electrode were in homogeneous media, halving its length should reduce the power required by 50%. The fact that the power requirement for the 5 mm electrode drops some 60-80% in vivo documents that the proximal portion of the 10 mm electrode is surrounded by tissue that is much more conductive than the tissue surrounding the distal half. The lower input heat with the shorter electrode may be more than enough, given that the heat is restricted to a small amount of tissue in a well-insulated compartment. The prevailing attitude is usually that as much heat as possible should be applied during the procedure, although this may be incorrect as discussed later. There are 2 general ways to increase RF heat production around the MB with a 5 mm electrode. First, RF current flow and subsequent heat dissipation around the electrode can be facilitated by providing a larger conduction path with the optimal impedance, e.g., an injectate. Secondly, a higher RF voltage/current can be applied to the electrodes, increasing the power dissipated. If no shunting is present (skeletal muscle is removed from the circuit), and all current passes through the region of the medial branch, this is relatively straightforward, although skeletal muscle shunting obviously negates most of the value of this maneuver. Increased power would be added by raising the target temperature as high as possible without producing an EIDT fault.

The 5 mm RF electrode should be positioned entirely within the tissue between bone and the overlying epimysial connective tissue layer, in order to physically restrict the RF heat generated to this compartment with minimal heat losses to nontarget tissues. Lastly, no soft tissue should be interposed between the electrode and the MB. Even having the epimysium of the LTPL in between the electrode and the MB is devastating to RF heating (Fig. 26). One of Bogduk's biggest contributions may have been to recognize that the MB is vulnerable only where it is fully exposed, across the approximately middle 50% of the SAP (68).

If the above criteria are met, RF heat is restricted to the area of the MBTZ and heat loss is low, a large temperature rise should occur at the MB. Optimal electrode usage by these newer criteria should be associated with a higher impedance and relatively low power inputs, e.g., 1-3 W.

The ultimate goal for lumbar medial branch RFA is to develop a therapeutic technique that is close to 100% effective in ablating the target medial branch (21,103,104). This involves some combination of maximizing energy input, minimizing current flow/heating

in nontarget tissues, maximizing current flow/heating in target tissues, and minimizing heat loss from target tissues.

The protocol outlined above should be at least as effective, if not more effective, than most protocols in use. In contemporary lumbar MB RFA with 10 mm electrodes, the majority of the available current capacity of the electrode is noneffective secondary to heating nontarget tissues, particularly with perpendicular positioning. This is primarily related to several phenomena, separately and together, e.g., 360° current spread, proportional current flow, electrode contact with shunting tissue (skeletal muscle), etc. If these phenomena are prominent, direct RF heating is largely limited to areas less than 1-2 mm from the electrode surface. Even this distance may be excessive if the target tissue and electrode are separated by poorly conducting tissues (Figs. 7, 25, 26). Effective heating at greater distances is dependent on heat conduction and/or convection. Increasing RF intensity should still be attempted, and conditions favoring conduction/convection optimized. Perhaps the most obvious alteration of technique is increased heating times, both adding more heat to the area, allowing more time for conduction/convection to occur, and increased heating times lowering the CLT.

Direct physical contact between the conventional RF electrode and the MB is the optimal situation; heat transfer under these circumstances is the most efficient. Injectates may be of value as discussed in the section *The Effect of Injectates prior to RF Lesioning*.

Matching the conformation of the RF electrode to the base of the SAP may be difficult, but should be attempted where possible (Figs. 20 and 21).

Heat transfer can therefore be quite complex, with a stochastic element due to variables such as the presence or absence of conductive fluids around the electrode. This variability should be minimized with the injection of a suitable electrolyte solution immediately prior to RF exposure per the criteria of the section *The Effect of Injectates prior to RF Lesioning*. Under these conditions, lumbar RF ablation should be a reasonably reproducible technique, and with careful attention to detail, the stochastic elements of the procedure would be minimized.

At this point, it should be clear why the behavior of an RF electrode cannot be described with a few parameters in a simple table.

It is illustrative to examine a few calculations. An electrode dissipating 10 W for 90 seconds produces 900 J of energy (W = J/s), which will raise the temperature of approximately 5 grams of water 42°C (900J ÷ [42 x 4.18 J/°-K]), approximately the rise involved with a target temperature of 80°C (37°C to 80°C). Heat losses are undoubtedly significant, and 900 J probably heats only 1 g-2 g of tissue to the target temperature, although only the CLT need be exceeded. Thermodynamic laws are never violated, and 900 J is a generous heat input for a lumbar RFR, probably occurring only when a 10 mm electrode is largely exposed to skeletal muscle, where much of the heat produced may not be utilized in heating the MB. Many times, the input is significantly less. Clearly, this heat must be distributed efficiently around the MB to produce a good lesion. The conclusion seems inescapable that suboptimal technique will rapidly degrade clinical outcomes.

These calculations also demonstrate the importance of limiting the heat loss of target tissues.

Based on the anatomy of the lumbar MB and its surroundings, both conventional and water-cooled electrodes are in a setting resembling hemicylindrical heating (55,81,83,84,97,105-108) (Figs. 20 and 26). Heat generation by the portion of the conventional RF electrode closest to the MB may not be high with either parallel or perpendicular positioning, although the electrode tip will be brought up to the target temperature regardless of this (32). Heating of the MB will be aided by the insulating effect of bone and connective tissue. If the electrode is positioned as in Fig. 4, most of the power dissipation will occur in skeletal muscle, a nontarget tissue.

This analysis implicitly brings up the very common misconception that the electrode should be positioned to achieve the minimum impedance possible. The minimum impedance will almost always be achieved with the electrode embedded purely in a low impedance, nontarget tissue. Low electrode impedance and high power inputs are "feel good" variables. The thermodynamic variables that matter are the ratio of target tissue heat input to the total heat capacity of the target tissues. The electrode should be positioned by anatomic and physiologic criteria, not by impedance values.

One of the reasons why Bogduk's positioning recommendations (8,11,13,56,70,76,77,109) have been so successful and widely accepted is that these recommendations achieve the above, with the exception that most operators use 10 mm electrodes (Fig. 17). An RF electrode based on a Sprotte-type needle would likely function better than the contemporary designs based on the Quincke-type needle, in terms of keeping the electrode in the plane between bone and soft tissue

without mechanically damaging the MB or piercing the epimysium of the overlying muscle.

Using focused stimulation to localize the MB in the anterior portion of the MBTZ, and then positioning the RF electrode by treating the problem as described in the section on RF electrode position, is likely the most accurate positioning technique, but positioning by purely anatomic criteria is probably almost as good. These 2 techniques need a rigorous comparison.

All too often, the effective zone of the RF electrode is visualized as being the same shape and size as the published PCS pictures from *in vitro* experiments, e.g., egg white. It must be repeated that the *in vivo* LZ absolutely cannot be represented by mapping the shape of an *in vitro* coagulum onto the end of the *in vivo* RF electrode because the shapes and sizes of the 2 lesion zones are virtually certain to be completely different. This is where tables of lesion size based on *in vitro* and *ex vivo* data reach their limit of usefulness.

Most discussion of lumbar RFR implies that the greater the amount of damage to the MB, the better. However, electromyographic and post-RFR imaging data would indicate that RFR is not the equivalent to transection of the MB (110). Electromyographic signs of denervation after RFR usually resolve (7,110), and no persistent marked atrophy of the multifidus muscles occurs; both findings are the opposite of what would occur with physical nerve transection (111). While Dreyfuss et al (111) found multifidus atrophy following RFR, the blinded radiologists interpreting the magnetic resonance images could not identify the side or level of the RFR, so that this atrophy had to have an etiology other than the RFR. The prognosis for MB recovery following a complete physical transection at the level of the SAP is poor. This suggests that clinical results are based on thermal damage to the MB or its vascular supply, or damage to nonaxonal cells, e.g., Schwann cells, which induces some long-lasting dysfunction of sensory transmission, e.g., dysfunctional re-myelination, etc. This is a well-known phenomenon in disorders such as predominantly demyelinating forms of Guillain-Barré Syndrome.

This raises the question of how important the length of the lesion is, since the impairment of sensory coding by dysfunctional re-myelination and temporal dispersion of sensory action potentials should be length dependent. At present, there are no data allowing one to accurately predict the length of the MB lesion in humans. The data presented suggest a shorter RF electrode will be more effective in lesioning, but it does not provide information on the relative length of the lesion relative to contemporary techniques. While in this respect the 10 mm electrode initially seems preferable over the 5mm electrode, the reader should appreciate that the length of the lesion may not correlate well with the length of the electrode. This is another area where additional basic study is needed. The author would predict that the goal of RFR is a primarily demyelinating lesion that is as long as possible, not a short axonotmetic lesion. The technique of "stacking" lesions "head-to-tail" needs to be investigated systematically. Multiple lesions are usually applied in a "side-by-side" fashion, which may not be optimal, particularly if the first lesion is done well.

A priori, one would assume that permanent denervation of the multifidus muscles is undesirable, and conditions favorable for neuroma formation should be avoided. This creates the possibility that as our RFR technique improves, MB damage may become excessive, and more precise control of RFR protocols will become a critical issue.

Analysis of the current literature, albeit essentially nonexistent, does not provide any support for physical transection of the MB, which could easily be done with a contemporary RF electrode, but in fact, is probably a complication to be avoided.

The current "gold standard" for documenting a successful MB RFR is clinical relief of back pain, although a better indicator is needed. This will most likely be some type of electrophysiologic study, e.g., needle electromyography, somatosensory potentials, etc. Pre-RFR baseline studies will probably be necessary. A well validated, easily obtained marker of clinically useful MB damage that could be evaluated shortly after RFR would be extremely valuable.

Progress is seriously hampered by the lack of a good *in vitro* test model for electrodes as well. The anatomy and tissue composition surrounding the human MB is unique and there are no good animal models. Some alternative to clinical results is needed since a clinical treatment and evaluation cycle takes so long to perform and has so many uncontrolled variables. Experimental systems such as those represented in Figs. 10 and 26 are probably best, noting that their value comes primarily from observing electrode behavior at boundaries, e.g., skeletal muscle/adipose tissue, skeletal muscle/bone, etc. Data obtained lesioning large volumes of homogenous tissue without interfaces between different types of tissue are not likely to be of great additional value to the literature.

The common protocol of heating for 90 seconds at 80°C needs to be re-evaluated in that there is significant data and theory that suggest that better results may be obtained with higher total heat inputs, e.g., from longer heating times and/or higher target temperatures. Higher target temperatures and larger RF electrodes are almost always effective ways, within limits, to increase power input with a given RF generator. Water-cooled RF electrodes are appropriate at times, but not always.

Several factors favor the use of the largest diameter electrode possible and are covered in the section *The Diameter of the RF Electrode*. Some clinicians feel that the larger electrodes result in greater postprocedure pain. However, it seems illogical to risk reducing the long-term effectiveness of an expensive and time-consuming procedure to avoid what is usually a minor or nonexistent problem. Even with relatively small electrodes, e.g., 22G, some patients report significant postprocedure pain, so small diameter electrodes only lower, not eliminate, the probability of postprocedure pain.

Large electrodes are certainly problematic if placed without anesthesia, and this is a good argument against using them in this fashion, especially since the patient's pain response will interfere with good electrode positioning. Techniques that utilize anesthesia during RF electrode placement eliminate this issue. The RF electrode should be positioned using local anesthesia after the desired position and angles of the RF electrode have been determined by anatomic criteria with or without focused electrical stimulation. The procedure can be made virtually painless if anesthetic is infiltrated while the electrode is placed, especially if pure anatomic positioning is used.

There are minor relative contraindications to larger electrodes in patients with impaired coagulation. While this rarely precludes their use, clinical judgment must be used. Smaller electrodes can certainly be used here, realizing that this significantly reduces the margin of error for electrode placement.

There are therefore multiple objective, data-supported reasons why larger electrodes should be more effective than smaller electrodes, and in the author's opinion, only subjective, "soft" arguments disfavoring the use of larger electrodes unless the RF electrode is placed without anesthesia or a coagulopathy is present.

As with the conventional RF electrode, a comprehensive discussion of the water-cooled RF electrode is not straightforward either. The water-cooled RF electrode has been advertised as being effective in lumbar RFR when used perpendicular to the nerve. This would certainly be desirable, in that the perpendicular approach is usually faster and easier than the parallel approach. However, it has not been documented beyond a reasonable doubt that perpendicular positioning of the water-cooled RF electrode in an environment of hemispherical heating creates adequate thermal damage of the MB even if tip heating appears quite impressive *in vitro* in PCS (112). Most of the heating in this position will involve nontarget tissue. This is clearly a case where one should not extrapolate *in vitro* PCS results to *in vivo* situations until validated by independent techniques (Figs. 10 and 26).

Under conditions more frequently seen in oncology and cardiology applications, the water-cooled RF electrode clearly makes a much larger lesion in target tissue. However, when the dimensions of the target tissue approach those of the electrode, as is the case with lumbar RFR, the conventional RF electrode actually produces higher temperatures very close to the electrode until the crossover distance shown in Fig. 24. This behavior makes it difficult to predict what is going to happen "close" to the water-cooled RF electrode with either parallel or perpendicular positioning. Bone adjacent to the water-cooled RF electrode creates the same issues as with conventional RF electrodes.

More research on, and undoubtedly modifications of, the water-cooled RF electrode system are needed before IPM likely benefits as much from water-cooling as have cardiology and oncology.

The final LZ can be increased in size with both conventional and water-cooled electrodes using multiple overlapping heating cycles until the size of the predicted LZ is adequate. As noted, this usually implies "side-by-side" positioning, but "head-to-tail" positioning needs to be considered as well. Even after local anesthetic has been introduced, repeat lumbar RFA can be performed several times in a given area with minor changes in electrode position. If the electrode is carefully and properly positioned by anatomic criteria for lumbar RFR in a lumbar spine that is not highly deformed, there should be no physiologically important structures within the lesioning range of the conventional RF electrode. Rare exceptions to this rule may occur in highly deformed spines. Repeat RF heating after anesthesia may not be safe in all locations of the body, and clinical judgment must be used.

While there are significant gaps in our understanding of RFA, it is important to understand what is already known, in order to form and test hypotheses to advance

our knowledge. It cannot be emphasized enough that RFA is not a "fully mature" technique by any measure, and there are numerous potential improvements that should lead to better clinical outcomes. Even with the reservations expressed herein about contemporary water-cooled electrodes for lumbar RFR, a new generation of water-cooled RF electrode systems designed specifically for IPM may turn out to be much more effective than contemporary conventional and water-cooled RF electrodes.

To accommodate our patients' needs for treatment of chronic pain amenable to RFA, we will need to be assisted in the future by improved equipment (113) and techniques. Until that time, we must extract the maximum performance possible from existing technologies, aided in part by a thorough understanding of the fundamental science underlying their application. This must also be done in an environment, at least in the US, where reimbursement is severely decreased, the funds normally used for capital equipment are largely being diverted to electronic medical records and other expenses associated with the changing nature of medicine, and no significant increase in equipment or expendable costs can be absorbed by physicians.

Acknowledgments:

I wish to thank Dr. Nikolai Bogduk, MD, PhD, DSc for reviewing the manuscript and serving as an invaluable resource when obscure anatomical questions arose.

I also wish to thank the International Spine Intervention Society for permission to reproduce copyrighted material.

Lastly, I am deeply ingratiated to Dr. James W. Albers, MD, PhD and Dr. Daniel T. Barry, MD, PhD for their invaluable assistance in final reviewing and editing of the manuscript, without which my life would have been far more difficult.

Appendix A

Definitions

Summary of Heat Equations: To discuss RF electrode function in more detail, some basic terminology used to discuss heat must be reviewed. Heat, measured in Joules (J), is synonymous with energy in this setting, and is usually represented by the symbol Q. Power is the rate at which energy is delivered to the tissue, $P = Z * j^2$, where Z is the impedance of the tissue through which the current passes, and j is the current density in the tissue (milliamperes/cm^2). Mathematically, energy can be expressed as the product of time (t) and power, $Q = P * t \equiv Z * j^2 * t$. Temperature largely reflects the kinetic energy of particles at the molecular level, and is independent of the amount of matter present. Temperature is related to the amount of energy present per unit of tissue and adding energy to tissue results in a temperature rise. The relationship between the amount of heat added and the tissue temperature increase is determined by the tissue's specific heat capacity (C_n), defined as the amount of energy required to raise the temperature of one gram of a substance by 1°C, e.g., the specific heat capacity of water = 4.184 J/gm-°C. The total tissue mass (m) and specific heat capacity (116) are multiplied together to obtain the total heat capacity of the tissue sample. Combining the above equations, we arrive at a formula for the temperature rise in a tissue element subjected to electrical energy addition, $\Delta T = \frac{Z * j^2 * t}{C_q * m}$

Body-Tissue Interface (BTI): The area of contact between the peripheral extent of the peri-electrode tissue of an electrode subunit and the rest of the body, arbitrarily defined as the location where extending the peri-electrode tissue any further has relatively little effect on the properties of the electrode subunit.

Conductive Heating: Heat conducted directly from a hotter object to a cooler object, purely on the basis of the temperature difference between the 2 objects.

Conventional Radiofrequency Electrode: A 16 – 22 gauge catheter, which is essentially a single lumen Quinke-type spinal needle, into which an RF generator probe is placed, with the probe extending to the distal tip of the needle. A temperature-sensing element, either a thermistor or thermocouple, is located in the very end of the probe, and feeds the temperature back to the RF generator where the generator adjusts the power input to the probe such that the target temperature is maintained at the temperature-sensing element. The cannula of the needle is coated with Teflon with the exception of the distal tip, where 2.5mm, 5mm, or 10mm of the bare metal cannula is left exposed for conventional electrodes and 4.5mm – 5.5mm for water-cooled RF electrodes. This exposed metal tip is the electrode actually referred to when discussing electrical and thermal properties. The Teflon-covered portion of

the electrode cannula plays little role in the electrothermal function of the electrode other than being electrically insulated.

Critical Lesioning Temperature (CLT): The temperature required to damage the target tissue to the point where biological dysfunction lasts long enough to be clinically valuable, with permanent cessation of biological function usually being the goal. This is not a single temperature, but a time temperature curve, e.g. the absolute lowest lethal temperature might require 1 – 2 hours of exposure whereas near the higher limit of lethal temperatures, a few milliseconds might be sufficient.

Current Density ($\mathbb{J}$): The amount of current flowing through a given region divided by the cross-sectional area of that region.

Effective Heat: That heat produced by the RF system that heats the target tissue and contributes to the desired clinical effect. This is in contrast to "ineffective heat" defined below.

Electrode, electrode surface, electrode diameter, ETI, electrode length, etc., all refer exclusively to the bare metal, electrically active exposed tip of the overall electrode.

Electrode Interface Disruption Temperature (EIDT): The temperature at which boiling and/or charring of the tissue around the electrode occurs, disrupting the electrical function of the RF electrode. It is the EIDT that usually limits the maximum intensity of the RF signal.

Electrode Subunit (ES): A volume of peri-electrode tissue which is delineated proximally at the electrode surface by the ETI, and peripherally at the distal end of the subunit by the tissue-body interface. When all the ES associated with an RF electrode are added together, much like a 3D puzzle, the resultant object is the overall RF electrode complex. The concept of the ES is introduced to explain electrode behavior when not all the peri-electrode tissue volumes around an electrode behave in the same manner electrically.

Electrode-Tissue Interface (ETI): The area of contact between the metal of the electrode surface and the peri-electrode tissue, where the electrical and chemical events associated with charge transfer between the 2 entities occurs.

Electroporation: A well-known phenomenon whereby the membrane of cells are damaged by an excessively high voltage gradient (V/cm) across the outer membrane. Damage is generally a function of the magnitude of the voltage gradient and the time the gradient is applied. With mild conditions, electroporation may be reversible, and has found many applications in molecular biology. If the voltage gradient and the time applied exceed critical limits, electroporation is irreversible, i.e., lethal to the cell.

Focused Stimulation: Stimulation with a small, e.g., 25ga – 30ga Teflon-covered needle with at most 1mm – 2mm of the tip exposed.

Generator Fault: Essentially all medical RF generators are designed to automatically shut down if conditions are detected that suggest a problem, e.g. impedance or power input outside the allowed range, temperature rise too rapid or slow for the power input present, etc. The ability to "fault" is intended to maximize patient safety, but sometimes interferes with legitimate uses of the generator.

Impedance: The all-encompassing term defined to describe the resistance of a circuit to current flow that covers both alternating current (AC) and direct current (DC) and is usually represented by the symbol $\mathbb{Z}$. The familiar "Ohm's Law," covers impedance for DC current, known simply as resistance. For AC current, the properties of inductance, which increases the resistance to current flow with increasing signal frequency, and capacitance, which decreases the resistance to current flow with increasing signal frequency must also be considered. Also, phase shift must be considered in many situations, which is where the AC current may lead or lag the AC voltage, whereas for DC, current and voltage are always synchronized, i.e., they are "in phase." Lastly, when the phase shift is not zero, the "Power Factor" may affect the amount of power transmitted. In this article, we will use "impedance" to emphasize that this is the correct term, but will treat impedance as a "resistance" to simplify things. We will avoid delving into the complexities introduced by a rigorous treatment of impedance.

Ineffective Heat: Heat produced by the RF signal that heats non-target tissue, and does not heat target tissue. Ineffective heat is a major problem in that it frequently uses a majority of the capacity of the RF system to heat tissue without contributing to lesioning the medial branch. Examples of ineffective heat include heating tissue that does not need to be heated or heating target tissue far beyond the point needed to create a lesion.

Lesioning Zone (LZ): The volume of tissue around the ablation electrode where the temperature-time product during a heating cycle is sufficient to cause a lesion to the enclosed tissue. (See "Critical Lesioning Temperature").

Maximum Temperature Zone (MTZ): The zone of tissue at the highest temperature during the equilibrium phase of an RF heating cycle. Boiling/charring will occur in the MTZ first if heating is excessive.

Medial Branch (MB): The term "medial branch" as used herein will implicitly include the medial branch proper, but also include small sensory nerves innervating the zygapophyseal joints that are actually branches of the medial branch, but whose ablation contributes to the clinical response.

Medial Branch Sulcus (MBS): The intersection of the transverse process (TP) and superior articular process (SAP) of a lumbar vertebra, along which the medial branch passes from anterior to posterior, entering anteriorly through an aperture in the medial aspect of the intertransversarii muscles and exiting posteriorly under the Mammillo-Accessory ligament between the mammillary process and the accessory process (Fig. 17).

Medial Branch Target Zone (MBTZ): The section of the medial branch superimposed on the middle one half of the SAP (25% – 75% of AP dimension in lateral radiograph, neglecting parallax errors unless extreme) in a lateral radiograph which is most suitable for RF electrode placement, as defined by Bogduk (73). The medial branch is essentially physically bare in this section without barriers to electrical flow.

MKS: The meter-kilogram-second, or "Metric" system.

Shunting: Current passing through multiple impedances in a parallel circuit divides itself between the individual impedances inversely proportional to the individual impedances. When one of the parallel impedances is particularly low relative to the other impedances, most of the current in the circuit will pass through the lowest impedance. That markedly low impedance is said to be "shunting" the circuit.

Target Temperature: The lesion temperature set in the RF generator, which originally was thought to represent the temperature of the entire electrode surface at equilibrium, although in reality, it represents only the temperature of the temperature-sensing element in the RF probe located inside the electrode cannula, and the tissue temperature may, and almost always does, differ significantly, particularly around the proximal electrode. Thermocouple and thermistor are used interchangeably since they are functionally equivalent to temperature sensor for the purposes of this article without discussing the electronic differences.

Water-Cooled Radiofrequency Probe: A probe that is identical to the conventional probe described above, with the exception that the probe has a triple lumen. One lumen is used to pass the RF probe as described above. The other lumens are used as the inflow and outflow channels for water through the cannula such that the entire active bare metal tip is cooled. The extent of cooling is determined by the temperature and the flow rate of the water. The goal of this cooling is to prevent temperature related disruption of the ETI, i.e., prevent reaching the EIDT. The goal of cooling is not complete homogeneity of temperature across the entire electrode.

Appendix B

Engineering Formulas

Conductivity: The reciprocal of resistivity with units of "Siemens." Likewise, when adjusted for the physical dimensions of the material, gives Conductance.

Energy = An extensive quantity where $Q = P \cdot t$, "energy" and "heat" are generally synonymous under most circumstances. Energy added or removed from a system is equal to power entering/leaving the system integrated as a function of time, e.g., Power x Time.

Heat Modeling Equations = Most problems involving electrical heating will be modeled to represent the manner in which current spreads out from its source. Two situations are common, current spreading out from a point source in a near spherical fashion, and current spreading out from a wire in a near cylindrical fashion. Heating at a given distance, *r*, from the source, will be proportional to current density, j^2 in either case. For a sphere, j^2 falls off as a function of $\frac{1}{r^4}$, while for a cylinder, j^2 falls off as a function of $\frac{1}{r^2}$. In almost all the RFA procedures performed in IPM, the electrode is best represented by a cylinder, and heating falls off as a function of $\frac{1}{r^2}$. Spherical models are largely restricted to the electrode environments found in cardiac and oncology procedures

Ohm's Law = $V = I \cdot R$. Derivatives of Ohm's law include $R = \frac{V}{I}; I = \frac{V}{R}; P = R \cdot I^2; P = V \cdot I \ (or\ E \cdot I)$. This version of Ohm's law applies only to DC current. A general form for AC current would be $V = I \cdot Z$, where Z is the complex impedance or $V = Z \cdot J$, where the current density, J, is substituted for I. To simplify explanations, no attempts to correct for phase angle or power factor will be made in this review.

Power P= The INSTANTANEOUS rate at which energy is delivered to, or dissipated by, a system, given by $P = R \cdot I^2$ for DC current and $P = Z * j^2$ for AC current, corrected for power factor, if necessary.

Resistive or Joule Heating = Heat produced electrically by effects for the DC case, and for the general case.

Resistivity = The resistivity of a material to the flow of electrical current, an intrinsic property of the material under consideration, e.g., copper, bone, muscle, etc., and when corrected for the dimensions of the object, $R = \frac{\rho \cdot l}{A}$ yields "resistance,", denoted by R.

Specific Heat Capacity ="C" is the amount of energy that must be added to a specific mass of material, e.g., one gram, to produce a temperature change of 1°C, e.g., $\Delta T = \frac{Q}{C_0} = \frac{Pt}{C_0}, or\ C_0 = \frac{Q}{\Delta T}$. For a homogeneous material, the "heat capacity," aka "total heat capacity" of a system is simply the specific heat capacity multiplied by the mass of the system, i.e., $\Delta T = \frac{Q}{C_0 x M} = \frac{Pxt}{C_0 x M}$ where the total mass of the material.

Thermal Conductivity = This is the rate at which heat is transferred across a structure, given by $Q = (k \cdot A \cdot \Delta T)/d$ where k = thermal conductivity, A = cross-sectional area, d = thickness, and ΔT = temperature difference across the structure.

References

1. Wood M, Huang S (eds). *Catheter Ablation of Cardiac Arrhythmias.* Saunders Elsevier, Philadelphia, PA, 2011.
2. Kwan KG, Matsumoto ED. Radiofrequency ablation and cryoablation of renal tumours. Curr Oncol 2007; 14:34-38.
3. Nath S, DiMarco JP, Haines DE. Basic aspects of radiofrequency catheter ablation. *J Cardiovasc Electrophysiol* 1994; 5:863-876.
4. Nath S, Haines DE. Biophysics and pathology of catheter energy delivery systems. Prog Cardiovasc Dis 1995; 37:185-204.
5. Syvanthong C, Wile GE, Zagoria RJ. Effect of radiofrequency ablation of renal tumors on renal function in patients with a solitary kidney. *AJR Am J Roentgenol* 2007; 188:1619-1621.
6. Liu Z, Lobo SM, Humphries S, Horkan C, Solazzo SA, Hines-Peralta AU, Lenkinski RE, Goldberg SN. Radiofrequency tumor ablation: Insight into improved efficacy using computer modeling. *AJR Am J Roentgenol* 2005; 184:1347-1352.
7. Dreyfuss P, Halbrook B, Pauza K, Joshi A, McLarty J, Bogduk N. Efficacy and validity of radiofrequency neurotomy for chronic lumbar zygapophysial joint pain. *Spine (Phila Pa 1976)* 2000; 25:1270-1277.
8. Van Kleef M, Weber WE, Kessels A, Dreyfuss P, Pauza K, Bogduk N. Re: Efficacy and validity of radiofrequency neurotomy for chroniclumbar zygapophysial joint pain (Spine 2000;25:1270-7). *Spine (Phila Pa 1976)* 2001; 26:E163-E164.
9. Lord SM, Bogduk N. Radiofrequency procedures in chronic pain. Best Pract Res Clin Anaesthesiol 2002; 16:597-617.
10. Bogduk N. On diagnostic blocks for lumbar zygapophysial joint pain. F1000 Med Rep 2010; 2:57.
11. Bogduk N. Lumbar radiofrequency neurotomy. Clin J Pain 2006; 22:409.
12. Bogduk N. The innervation of the lumbar spine. *Spine (Phila Pa 1976)* 1983; 8:286-293.
13. Bogduk N. Evidence-informed management of chronic low back pain with facet injections and radiofrequency neurotomy. *Spine J* 2008; 8:56-64.
14. Nath S, Nath CA, Pettersson K. Percutaneous lumbar zygapophysial (facet) joint neurotomy using radiofrequency current, in the management of chronic low back pain: A randomized double-blind trial. *Spine (Phila Pa 1976)* 2008; 33:1291-1297; discussion 1298.
15. Leclaire R, Fortin L, Lambert R, Bergeron YM, Rossignol M. Radiofrequency facet joint denervation in the treatment of low back pain: A placebo-controlled clinical trial to assess efficacy. *Spine (Phila Pa 1976)* 2001; 26:1411-1416; discussion 1417.
16. van Kleef M, Vanelderen P, Cohen SP, Lataster A, Van Zundert J, Mekhail N. 12. Pain originating from the lumbar facet joints. *Pain Pract* 2010; 10:459-469.
17. Van Zundert J, Mekhail N, Vanelderen P, van Kleef M. Diagnostic medial branch blocks before lumbar radiofrequency zygapophysial (facet) joint denervation: Benefit or burden? *Anesthesiology* 2010; 113:276-278.
18. Van Zundert J, Vanelderen P, Kessels A, van Kleef M. Radiofrequency treatment of facet-related pain: Evidence and controversies. *Curr Pain Headache Rep* 2012; 16:19-25.
19. Slipman CW, Bhat AL, Gilchrist RV, Issac Z, Chou L, Lenrow DA. A critical review of the evidence for the use of zygapophysial injections and radiofrequency denervation in the treatment of low back pain. Spine J 2003; 3:310-316.
20. Datta S, Lee M, Falco FJ, Bryce DA, Hayek SM. Systematic assessment of diagnostic accuracy and therapeutic utility of lumbar facet joint interventions. *Pain Physician* 2009; 12:437-460.
21. Falco FJ, Manchikanti L, Datta S, Sehgal N, Geffert S, Onyewu O, Singh V, Bryce DA, Benyamin RM, Simopoulos TT, Vallejo R, Gupta S, Ward SP, Hirsch JA. An update of the systematic assessment of the diagnostic accuracy of lumbar facet joint nerve blocks. *Pain Physician* 2012; 15:E869-907.
22. Manchikanti L, Benyamin RM, Falco, FJE, Caraway DL, Datta S, Hirsch JA. Guidelines warfare over interventional techniques: Is there a lack of discourse or straw man? *Pain Physician* 2012; 15:E1-E26.
23. Klessinger S. Radiofrequency neurotomy for treatment of low back pain in patients with minor degenerative spondylolisthesis. *Pain Physician* 2012; 15:E71-E78.
24. Cosman E, Dolensky J, Hoffman R. Factors That Affect Radiofrequency Heat Lesion Size. www.painmed.org/2013posters/abstract-102/
25. Cosman ER, Jr., Cosman ER, Sr. Electric and thermal field effects in tissue around radiofrequency electrodes. *Pain Med* 2005; 6:405-424.
26. Chen W, Lee RC. Altered ion channel conductance and ionic selectivity induced by large imposed membrane potential pulse. *Biophys J* 1994; 67:603-612.
27. Garcia PA, Pancotto T, Rossmeisl JH, Jr., Henao-Guerrero N, Gustafson NR, Daniel GB, Robertson JL, Ellis TL, Davalos RV. Non-thermal irreversible electroporation (N-TIRE) and adjuvant fractionated radiotherapeutic multimodal therapy for intracranial malignant glioma in a canine patient. *Technol Cancer Res Treat* 2011; 10:73-83.
28. Hofmann GA, Dev SB, Nanda GS, Rabussay D. Electroporation therapy of solid tumors. *Crit Rev Ther Drug Carrier Syst* 1999; 16:523-569.
29. Lee TH, Yang LC, Chou AK, Wu PC, Lin CR, Wang CH, Chen JT, Tang CS. In vivo electroporation of proopiomelanocortin induces analgesia in a formalin-injection pain model in rats. *Pain* 2003; 104:159-167.
30. Rubinsky B, (ed). I*rreversible Electroporation. Series in Biomedical Engineering.* Springer-Verlag, Berlin-Heidelberg, 2010.
31. Yuan TF. Electroporation: An arsenal of application. *Cytotechnology* 2007; 54:71-76.
32. Haines DE. *Biophysics of Radiofrequency Lesion Formation.* Saunders Elsevier, Philadelphia, PA, 2011, pp 2-19.
33. Malik K, Benzon HT, Walega D. Water-cooled radiofrequency: A neuroablative or a neuromodulatory modality with broader applications? *Case Rep Anesthesiol* 2011; 2011:263101.
34. Karaman H, Tufek A, Kavak GO, Kaya S, Yildirim ZB, Uysal E, Celik F. 6-month results of transdiscal biacuplasty on patients with discogenic low back pain: Preliminary findings. *Int J Med Sci* 2010; 8:1-8.
35. Kapural L, Mekhail N. Novel intradiscal biacuplasty (IDB) for the treatment of lumbar discogenic pain. *Pain Pract* 2007; 7:130-134.
36. Kapural L. Intervertebral disk cooled bipolar radiofrequency (intradiskal biacuplasty) for the treatment of lumbar diskogenic pain: A 12-month follow-up of the pilot study. *Pain Med* 2008; 9:407-408.
37. Pauza K. Cadaveric intervertebral disc temperature mapping during disc biacuplasty. *Pain Physician* 2008; 11:669-676.
38. Haemmerich D, Chachati L, Wright AS, Mahvi DM, Lee FT, Jr., Webster JG. Hepatic radiofrequency ablation with internally cooled probes: Effect of coolant

temperature on lesion size. *IEEE Trans Biomed Eng* 2003; 50:493-500.

39. Tatli S, Tapan U, Morrison PR, Silverman SG. Radiofrequency ablation: Technique and clinical applications. *Diagn Interv Radiol* 2012; 18:508-516.
40. Golio JM. *The RF and Microwave Handbook: RF and Microwave Circuits, Measurements, and Modeling.* CRC Press, Boca Raton, FL, 2008.
41. Northover BJ. Electrical Properties of Mammalian Tissues: An Introduction. Chapman & Hall, London, 1992.
42. Newman JS, Thomas-Alyea KE. *Electrochemical Systems.* J. Wiley, Hoboken, NJ, 2004.
43. Hamann CH, Hamnett A, Vielstich W. *Electrochemistry*. Wiley-VCH, Weinheim, 1998.
44. Herman SL, Duff JR. *Alternating Current Fundamentals.* Delmar Cengage Learning, Clifton Park, NY, 2011.
45. Ida N. *Engineering Electromagnetics.* Springer, New York, 2004.
46. Atkins PW, De Paula J. *Physical Chemistry*. W.H. Freeman, New York, 2010.
47. Bergman TL, Incropera FP. *Fundamentals of Heat and Mass Transfer.* Wiley, Hoboken, NJ, 2011.
48. Hazen ME. *Fundamentals of DC and AC circuits.* Saunders College Pub, Philadelphia, 1990.
49. Ward E, Munk PL, Rashid F, Torreggiani WC. Musculoskeletal interventional *Radiology*: Radiofrequency ablation. *Radiol Clin North Am* 2008; 46:599-610, vi-vii.
50. Gileadi E. *Electrode Kinetics for Chemists, Chemical Engineers, and Materials Scientists*. VCH, New York, 1993.
51. Pletcher D; Royal Society of Chemistry (Great Britain). *A First Course in Electrode Processes.* Royal Society of Chemistry, Cambridge, 2009.
52. Haines DE, Verow AF. Observations on electrode-tissue interface temperature and effect on electrical impedance during radiofrequency ablation of ventricular myocardium. *Circulation* 1990; 82:1034-1038.
53. McRury ID, Panescu D, Mitchell MA, Haines DE. Nonuniform heating during radiofrequency catheter ablation with long electrodes: Monitoring the edge effect. *Circulation* 1997; 96:4057-4064.
54. Solazzo SA, Ahmed M, Liu Z, Hines-Peralta AU, Goldberg SN. High-power generator for radiofrequency ablation: Larger electrodes and pulsing algorithms in bovine *ex vivo* and porcine in vivo settings. *Radiology* 2007; 242:743-750.
55. Solazzo SA, Liu Z, Lobo SM, Ahmed M, Hines-Peralta AU, Lenkinski RE, Goldberg SN. Radiofrequency ablation: Importance of background tissue electrical conductivity--an agar phantom and computer modeling study. *Radiology* 2005; 236:495-502.
56. Bogduk N, Macintosh J, Marsland A. Technical limitations to the efficacy of radiofrequency neurotomy for spinal pain. *Neurosurgery* 1987; 20:529-535.
57. Haines DE, Watson DD, Verow AF. Electrode radius predicts lesion radius during radiofrequency energy heating. Validation of a proposed thermodynamic model. *Circ Res* 1990; 67:124-129.
58. Letcher FS, Goldring S. The effect of radiofrequency current and heat on peripheral nerve action potential in the cat. *J Neurosurg* 1968; 29:42-47.
59. Smith HP, McWhorter JM, Challa VR. Radiofrequency neurolysis in a clinical model. Neuropathological correlation. *J Neurosurg* 1981; 55:246-253.
60. Lu DS, Raman SS, Vodopich DJ, Wang M, Sayre J, Lassman C. Effect of vessel size on creation of hepatic radiofrequency lesions in pigs: Assessment of the "heat sink" effect. *AJR Am J Roentgenol* 2002; 178:47-51.
61. Goldberg SN, Hahn PF, Tanabe KK, Mueller PR, Schima W, Athanasoulis CA, Compton CC, Solbiati L, Gazelle GS. Percutaneous radiofrequency tissue ablation: Does perfusion-mediated tissue cooling limit coagulation necrosis? *J Vasc Interv Radiol* 1998; 9:101-111.
62. Liu Z, Ahmed M, Weinstein Y, Yi M, Mahajan RL, Goldberg SN. Characterization of the RF ablation-induced "oven effect": The importance of background tissue thermal conductivity on tissue heating. *Int J Hyperthermia* 2006; 22:327-342.
63. Bien T, Rose G, Skalej M. *FEM Modeling of Radio Frequency Ablation in the Spinal Column.* 3rd International Conference on Biomedical Engineering and Informatics (BMEI 2010), Yantai, China, Institute of Electrical and Electronics Engineers.
64. Haemmerich D, Schutt DJ. RF ablation at low frequencies for targeted tumor heating: In vitro and computational modeling results. *IEEE Trans Biomed Eng* 2011; 58:404-410.
65. Bogduk N, Long DM. The anatomy of the so-called "articular nerves" and their relationship to facet denervation in the treatment of low-back pain. *J Neurosurg* 1979; 51:172-177.
66. Bogduk N. A reappraisal of the anatomy of the human lumbar erector spinae. *J Anat* 1980; 131:525-540.
67. Bogduk N. Rhizolysis. *Anaesthesia* 1980; 35:1020.
68. Bogduk N, Long DM. Percutaneous lumbar medial branch neurotomy: A modification of facet denervation. *Spine (Phila Pa 1976)* 1980; 5:193-200.
69. Bogduk N. Lumbar lateral branch neuralgia: A complication of rhizolysis. *Med J Aust* 1981; 1:242-243.
70. Baker K, Bogduk N, Burnett I, Davis R, Jones D, Meldrum B, Munro R. Proceedings: Displacement of articular surfaces in the hip joint. *J Anat* 1973; 116:477.
71. Bogduk N. The lumbar mamillo--accessory ligament. Its anatomical and neurosurgical significance. *Spine (Phila Pa 1976)* 1981; 6:162-167.
72. Bogduk N, Wilson AS, Tynan W. The human lumbar dorsal rami. *J Anat* 1982; 134:383-397.
73. Bogduk N, Colman RR, Winer CE. An anatomical assessment of the "percutaneous rhizolysis" procedure. *Med J Aust* 1977; 1:397-399.
74. Mercer S, Bogduk N. The ligaments and annulus fibrosus of human adult cervical intervertebral discs. *Spine (Phila Pa 1976)* 1999; 24:619-626; discussion 627-618.
75. Bogduk N. Radiofrequency treatment in Australia. *Pain Pract* 2002; 2:180-182.
76. Bogduk N. In defense of radiofrequency neurotomy. *Reg Anesth Pain Med* 2002; 27:439-441; author reply 441-432.
77. Lau P, Mercer S, Govind J, Bogduk N. The surgical anatomy of lumbar medial branch neurotomy (facet denervation). *Pain Med* 2004; 5:289-298.
78. Bogduk N; International Spine Intervention Society Standards Committee. *Practice Guidelines for Spinal Diagnostic and Treatment Procedures.* International Spine Intervention Society, San Francisco, 2004.
79. Stanley PC, Pilkington TC, Morrow MN, Ideker RE. An assessment of variable thickness and fiber orientation of the skeletal muscle layer on electrocardiographic calculations. *IEEE Trans Biomed Eng* 1991; 38:1069-1076.
80. Stanley PC, Pilkington TC. The combination method: A numerical technique for electrocardiographic calculations. *IEEE Trans Biomed Eng* 1989; 36:456-461.
81. Williams PA, Saha S. The electrical and dielectric properties of human bone tissue and their relationship with density

and bone mineral content. Ann Biomed Eng 1996; 24:222-233.

82. Rachbauer F, Mangat J, Bodner G, Eichberger P, Krismer M. Heat distribution and heat transport in bone during radiofrequency catheter ablation. *Arch Orthop Trauma Surg* 2003; 123:86-90.
83. Panescu D, Whayne JG, Fleischman SD, Mirotznik MS, Swanson DK, Webster JG. Three-dimensional finite element analysis of current density and temperature distributions during radio-frequency ablation. *IEEE Trans Biomed Eng* 1995; 42:879-890.
84. Panescu D, Webster J. Effects of changes in electrical and thermal conductivities on radiofrequency lesion dimensions. Proceedings - 19th International Conference - IEEE/EMBS. Chicago, IL; 1997. IEEE. 1:154-157.
85. Rybak LD. Fire and ice: Thermal ablation of musculoskeletal tumors. *Radiol Clin North Am* 2009; 47:455-469.
86. Geddes LA, Baker LE. The specific resistance of biological material--a compendium of data for the biomedical engineer and physiologist. *Med Biol Eng* 1967; 5:271-293.
87. Dadd JS, Ryan TP, Platt R. Tissue impedance as a function of temperature and time. *Biomed Sci Instrum* 1996; 32:205-214.
88. Haemmerich D. Biophysics of radiofrequency ablation. *Crit Rev Biomed Eng* 2010; 38:53-63.
89. Bogduk N, Twomey LT. *Clinical Anatomy of the Lumbar Spine.* Churchill Livingstone, Melbourne,, 1987.
90. Macintosh JE, Bogduk N. 1987 Volvo award in basic science. The morphology of the lumbar erector spinae. *Spine (Phila Pa 1976)* 1987; 12:658-668.
91. Bogduk N, Macintosh JE, Pearcy MJ. A universal model of the lumbar back muscles in the upright position. *Spine (Phila Pa 1976)* 1992; 17:897-913.
92. Macintosh JE, Bogduk N. The attachments of the lumbar erector spinae. *Spine (Phila Pa 1976)* 1991; 16:783-792.
93. Hong KN, Russo MJ, Liberman EA, Trzebucki A, Oz MC, Argenziano M, Williams MR. Effect of epicardial fat on ablation performance: A three-energy source comparison. *J Card Surg* 2007; 22:521-524.
94. Ball R (ed). Electrodiagnostic Evaluation of the Peripheral Nervous System, 3rd ed. *Principles and Practices in Rehabilitation Medicine.* JB Lippincott Co, Philadelphia, PA, 1998.
95. Cohen SP, Strassels SA, Kurihara C, Lesnick IK, Hanling SR, Griffith SR, Buckenmaier CC, 3rd, Nguyen C. Does sensory stimulation threshold affect lumbar facet radiofrequency denervation outcomes? A prospective clinical correlational study. *Anesth Analg* 2011; 113:1233-1241.
96. Masini M, Paiva WS, Araujo AS, Jr. Anatomical description of the facet joint innervation and its implication in the treatment of recurrent back pain. *J Neurosurg Sci* 2005; 49:143-146; discussion 146.
7. Goldberg SN, Ahmed M, Gazelle GS, Kruskal JB, Huertas JC, Halpern EF, Oliver BS, Lenkinski RE. Radio-frequency thermal ablation with NaCl solution injection: Effect of electrical conductivity on tissue heating and coagulation-phantom and porcine liver study. *Radiology* 2001; 219:157-165.
98. Lobo SM, Liu ZJ, Yu NC, Humphries S, Ahmed M, Cosman ER, Lenkinski RE, Goldberg W, Goldberg SN. RF tumour ablation: Computer simulation and mathematical modelling of the effects of electrical and thermal conductivity. *Int J Hyperthermia* 2005; 21:199-213.
99. Ahmed M, Lobo SM, Weinstein J, Kruskal JB, Gazelle GS, Halpern EF, Afzal SK, Lenkinski RE, Goldberg SN. Improved coagulation with saline solution pretreatment during radiofrequency tumor ablation in a canine model. *J Vasc Interv Radiol* 2002; 13:717-724.
100. Provenzano DA, Liebert MA, Somers DL. Increasing the NaCl concentration of the preinjected solution enhances monopolar radiofrequency lesion size. *Reg Anesth Pain Med* 2013; 38:112-123.
101. Provenzano DA, Lutton EM, Somers DL. The effects of fluid injection on lesion size during bipolar radiofrequency treatment. *Reg Anesth Pain Med* 2012; 37:267-276.
102. Provenzano DA, Lassila HC, Somers D. The effect of fluid injection on lesion size during radiofrequency treatment. *Reg Anesth Pain Med* 2010; 35:338-342.
103. Falco FJ, Manchikanti L, Datta S, Sehgal N, Geffert S, Onyewu O, Zhu J, Coubarous S, Hameed M, Ward SP, Sharma M, Hameed H, Singh V, Boswell MV. An update of the effectiveness of therapeutic lumbar facet joint interventions. *Pain Physician* 2012; 15:E909-E953.
104. Cohen SP, Williams KA, Kurihara C, Nguyen C, Shields C, Kim P, Griffith SR, Larkin TM, Crooks M, Williams N, Morlando B, Strassels SA. Multicenter, randomized, comparative cost-effectiveness study comparing 0, 1, and 2 diagnostic medial branch (facet joint nerve) block treatment paradigms before lumbar facet radiofrequency denervation. *Anesthesiology* 2010; 113:395-405.
105. Binette JS, Garon M, Savard P, McKee MD, Buschmann MD. Tetrapolar measurement of electrical conductivity and thickness of articular cartilage. *J Biomech Eng* 2004; 126:475-484.
106. Gabriel C, Gabriel S, Corthout E. The dielectric properties of biological tissues: I. Literature survey. *Phys Med Biol* 1996; 41:2231-2249.
107. Gabriel S, Lau RW, Gabriel C. The dielectric properties of biological tissues: II. Measurements in the frequency range 10 Hz to 20 GHz. Phys Med Biol 1996; 41:2251-2269.
108. Roth B (ed). *The Electrical Conductivity of Tissues.* The Biomedical Engineering Handbook. CRC Press, LLC, Boca Raton, 2006.
109. Macvicar J, Borowczyk JM, Macvicar AM, Loughnan BM, Bogduk N. Lumbar medial branch radiofrequency neurotomy in New Zealand. *Pain Med* 2012; 14:639-645.
110. Oudenhoven R. Paraspinal electromyography following facet rhizotomy. *Spine (Phila Pa 1976)* 1977; 2:6.
111. Dreyfuss P, Stout A, Aprill C, Pollei S, Johnson B, Bogduk N. The significance of multifidus atrophy after successful radiofrequency neurotomy for low back pain. *PM R* 2009; 1:719-722.
112. Kimberly-Clark. Cooled Radiofrequency Products. http://kchealthcare.com/us/healthcare/home/products/pain-management/chronic-pain-solutions/cooled-radiofrequency-products.aspx
113. Berjano EJ, Navarro E, Ribera V, Gorris J, Alio JL. Radiofrequency heating of the cornea: An engineering review of electrodes and applicators. *Open Biomed Eng J* 2007; 1:71-76.
114. Chang IA, Nguyen UD. Thermal modeling of lesion growth with radiofrequency ablation devices. *Biomed Eng Online* 2004; 3:27.
115. McIntosh RL, Anderson V. A comprehensive tissue properties database provided for the thermal assessment of a human at rest. Biophysical Reviews and Letters 2010; 5:129-151.
116. Bernardi P, Cavagnaro M, Pisa S, Piuzzi E. Specific absorption rate and temperature elevation in a subject exposed in the far-field of radio-frequency sources operating in the 10-900-MHz range.

IEEE Trans Biomed Eng 2003; 50:295-304.

117. Ducharme MB, Frim J. A multicouple probe for temperature gradient measurements in biological materials. *J Appl Physiol* 1988; 65:2337-2342.
118. Ducharme MB, Frim J, Tikuisis P. Errors in heat flux measurements due to the thermal resistance of heat flux disks. *J Appl Physiol* 1990; 69:776-784.
119 Ducharme MB, Tikuisis P. In vivo thermal conductivity of the human forearm tissues. *J Appl Physiol* 1991; 70:2682-2690.
120. Ducharme MB, Tikuisis P. Role of blood as heat source or sink in human limbs during local cooling and heating. *J Appl Physiol* 1994; 76:2084-2094.
121. Ducharme MB, VanHelder WP, Radomski MW. Tissue temperature profile in the human forearm during thermal stress at thermal stability. *J Appl Physiol* 1991; 71:1973-1978.
122. Frim J, Ducharme MB. Heat flux transducer measurement error: A simplified view. *J Appl Physiol* 1993; 74:2040-2044.
123. McIntosh RL, Anderson V. SAR versus S(inc): What is the appropriate RF exposure metric in the range 1-10 GHz? Part II: Using complex human body models. *Bioelectromagnetics* 2010; 31:467-478.
124. McRury ID, Whayne JG, Haines DE. Temperature measurement as a determinant of tissue heating during radiofrequency catheter ablation: An examination of electrode thermistor positioning for measurement accuracy. *J Cardiovasc Electrophysiol* 1995; 6:268-278.
125. Spells K. The thermal conductivities of some biological fluids. *Physics in Medicine and Biology* 1960; 5:139.